Sādhanā (2021)46:162
https://doi.org/10.1007/s12046-021-01685-2

Additive manufacturing of ceramics and cermets: present status and future perspectives

MAINAK SAHA[1,2,*] and MANAB MALLIK[1,*]

[1]Department of Metallurgical and Materials Engineering, National Institute of Technology, Durgapur 713209, West Bengal, India
[2]Department of Metallurgical and Materials Engineering, Indian Institute of Technology, Madras 600036, Tamil Nadu, India
e-mail: mainaksaha1995@gmail.com; manab.mallik@mme.nitdgp.ac.in

MS received 6 November 2020; revised 19 May 2021; accepted 6 July 2021

Abstract. The present decade has witnessed a huge volume of research revolving around a number of Additive Manufacturing (AM) techniques, especially for the fabrication of different metallic materials. However, fabrication of ceramics and cermets using AM-based techniques mainly suffers from two primary limitations which are: (i) low density and (ii) poor mechanical properties of the final components. Although there has been a considerable volume of work on AM based techniques for manufacturing ceramic and cermet parts with enhanced densities and improved mechanical properties, however, there is limited understanding on the correlation of microstructure of AM-based ceramic and cermet components with the mechanical properties. The present article is aimed to review some of the most commonly used AM techniques for the fabrication of ceramics and cermets. This has been followed by a brief discussion on the microstructural developments during different AM-based techniques. In addition, an overview of the challenges and future perspectives, mainly associated with the necessity towards developing a systematic structure-property correlation in these materials has been provided based on three factors viz. the efficiency of different AM-based fabrication techniques (involved in ceramic and cermet research), an interdisciplinary research combining ceramic research with microstructural engineering and commercialisation of different AM techniques based on the authors' viewpoints.

Keywords. Selective Laser Sintering (SLS®); additive manufacturing (AM); Cermets; selective laser melting (SLM); stereolithography; correlative characterisation.

1. Introduction

The past decades have witnessed ceramics and cermets becoming the centre of attraction in material science especially owing to excellent properties, ranging from enhanced high-temperature strength to high-wear resistance at both room and elevated temperatures [1–6]. Although significant work has been done with the main aim of designing ceramics with enhanced mechanical properties, the major limitations are set especially by the structural complexity of ceramics, considering high-performance requirements in aerospace, defence, electronic, energy sectors, etc. [7–12]. Fabrication of complex ceramic and cermet parts poses severe challenges, especially in mould manufacturing process which tends to be costly and time-consuming through conventional forming techniques such as dry pressing, isostatic pressing, etc. [8, 13–15]. This has led to an ever-increasing demand for a novel forming method, in order to manufacture high-performance ceramic and cermet components with complex shapes. Selective laser sintering (SLS®), since its onset, has delivered promising results in direct fabrication of metals, polymers, ceramics, etc. [16]. Wu *et al* [17] have reported a technique for preparation of powder beds for direct SLS® using aerosol-assisted spray deposition of Al_2O_3 suspension. Usually, a conventional roller is used to deposit powder layers which are subsequently made to undergo local heating and sintering according to geometries (predefined using 3D Computer-Aided Design (CAD) data) using selective laser beam scanning. A heating system is then used to preheat powder bed during SLS® in order to reduce thermal stresses, minimising the chances of crack formation in sintered parts [18].

The main challenges associated with the use of SLS® for manufacturing high performance ceramics and cermets with complex shapes are: (i) Difficulty in manufacturing crack-free dense ceramic and cermet components using SLS owing to the extremely high melting points of these

*For correspondence
Published online: 10 August 2021

materials and (ii) Poor thermal shock resistance (associated with extremely high rates of heating and cooling during SLS) coupled with negligible plasticity of ceramics, leading to high chances of crack formation in these brittle materials. In the context of direct SLS®-fabricated ceramic parts, easy cracking is extremely difficult to avoid, primarily owing to thermal stresses during the sintering process, leading to poor mechanical properties of finished products [19]. A number of studies have highlighted that indirect SLS method may be used as an alternative method to densify ceramics and prevent cracking in these materials through sintering of polymer binders (with low melting points) with the ceramic powder compositions, subsequently followed by removal of the polymer binder with slow heating rate and finally, furnace sintering to densify the final product with minimal chances of crack formation [20].

Powder bed fusion processes have been described as additive manufacturing (AM)-based processes in which thermal energy undergoes selective fusion into zone of a powder bed [21]. Generally, a laser beam or an electron beam is utilized as the origin of thermal energy for irradiation of powder particles. However, till date, AM processes like Electron Beam Melting (EBM) have only been used for fabricating metal-matrix composites (MMCs) and not for ceramics [22]. As shown in table 1, the irradiation of powder particles by thermal energy (originating from a laser beam) may initiate a number of processes such as: complete or a partial melting of powder particles, solid state sintering of powder particles and gelation (formation of a 3D network that traps the powder particles) [23]. Moreover, if the powder particles are not fully melted by the laser beam, the process may be referred to as Selective Laser Melting (SLM). All other laser based powder bed fusion operations can be referred to as Selective Laser Sintering® (SLS®) process [24].

On the other hand, interfaces are 2-D defects which separate two crystals with difference in crystallographic orientation [25]. The structure coupled with the localised atomic arrangement at these interfaces play a vital role in measuring the overall mechanical response of a material [26]. The present decade has witnessed the evolution of "Correlative Microscopy" methodology which involves using multiple microscopy techniques in a given microstructure to obtain both structural and spectroscopic information [27–30]. Moreover, this technique has been widely employed to understand structure-property correlation in a number of metallic materials and has also been reported to provide a major development in the understanding of different interfaces in these materials. In other words, the present research in the field of AM mainly revolves around a number of metallic materials. However, there is a very little emphasis on understanding structure-property correlation in AM-based ceramics and cermets which exhibit a number of interesting properties. Most interestingly, AM-based techniques may be used to design complex-shaped ceramic and cermet components unlike the parts fabricated using conventional techniques [22]. Low density and poor mechanical properties arising due to microstructural heterogeneities may be attributed as the main reasons for limited investigations in AM-based ceramics and cermets [10–21].

To this end, the present review is aimed at discussing some of the common AM techniques (both conventional

Table 1. Overview of AM processes for fabrication of ceramics [22].

Classified by ISO/ASTM							Not yet classified by ISO/ASTM	
Single step	Multi-step							
Directed energy Deposition	Powder Bed Fusion	Vat photo-polymerisation	Material Jetting	Material Extrusion	Sheet Lamination	Binder Jetting	Electro-phoretic deposition	Electro-photographic printing

Powder Bed Fusion															
Multi-step/single step	Single-step												Multi-step		
Binding mechanism	Full melting			Partial melting					Solid-state sintering	Chemically induced binding			Partial melting		gelling
Powder deposition mechanism	conventional	Slurry coater	Aerosol-assisted spray deposition	conventional	Slurry-coating	Slurry sprayer	Ring blade	Electro-phoretic deposition	conventional	conventional	Slurry-coater	Ring-blade	conventional	Slurry-coater	Slurry coater

and advanced) for the fabrication of ceramics and cermets with complex geometries and a wide range of applications. Sections 2 and 3 highlight the conventional and advanced AM-based fabrication techniques (for ceramics), respectively. Section 4 discusses the recently-developed AM-based techniques for the fabrication of cermets. Moreover, a brief discussion (from both industrial and fundamental viewpoints) on the present status and future perspectives has been provided in section 5 with a special emphasis on the requirement for investigations based on structure-property correlation in AM-based ceramics and cermets. In section 5.1, challenges associated with AM of ceramics and cermets have been discussed from the viewpoint of different .AM-based fabrication techniques. In section 5.2, microstructural heterogeneities arising due to non-equilibrium processing conditions in AM-based techniques have been specially highlighted. The last section (section 5.3) of the present review highlights the perspectives and outlooks on AM of ceramics and cermets from the authors' viewpoint.

2. A few commonly used AM techniques for fabrication of ceramics

2.1 *Material jetting*

The material jetting methods which are used to shape ceramic components are as follows:

2.1.1 *Inkjet printing (IJP) (Direct) [31–34]:*

During this process, there is a direct deposition of a suspension of ceramic powder particles from a print nozzle (for depositing single droplets of the powder suspension) on a substrate. Upon contact between droplets and the substrate, the droplets undergo phase transformation to solid state.

2.1.2 *Aerosol jet printing (AJP) [35, 36]:*

In this technique, a suspension comprising of fine ceramic powders with droplets in a gaseous medium is used, unlike liquid ink droplets used as printing media in IJP technique.

2.2 *Material extrusion techniques*

The material extrusion techniques used to shape different ceramic components mainly include:

2.2.1 *Fused deposition of ceramics (FDC):*

FDC is referred to as multiphase jet solidification (MJS) or extrusion free forming (EFF) [22, 37, 38], has an advantage of being able to fabricate a wide variety of materials owing to similarities with metal injection molding (MIM) technique. However, the main limitations of the process are: (i) materials must possess a suitable viscosity (10-200 Pa.s), and (ii) melting temperature of the binder must be less than 200°C [31].

In the context of ceramics, powder particles ($\sim$ 60 vol.%) are initially dispersed into a thermoplastic filament (acting as a binder) followed by a subsequent layer by layer melting (partial) of the same filament and its extrusion from a moving deposition head onto a fixed worktable [22]. The powder-binder mixture is passed as a feedstock through the machine, where it is initially heated above its melting point (in order to achieve a suitable viscosity) and subsequently squeezed out of the nozzle by a pumping system for a layer by layer deposition. The molten material undergoes solidification once in contact with the platform [31].

2.2.2 *Robocasting [37–48]:*

In robocasting, also referred to as 3D fibre deposition (3DFD [41]) or Micropen [42–45], a concentrated sol is made to undergo extrusion through a nozzle so as to form a filament for a controlled layer by layer deposition to form 3D structures [22].

Unlike FDC (mentioned previously,) this method does not involve partial melting of the polymer. Freeze-Form Extrusion Fabrication (FEF) has been reported as a special Robocasting technique which involves deposition and subsequent freezing of a colloidal gel on a cooled substrate [22, 40]. This technique has been used to fabricate Al_2O_3 by Leu *et al* [47]. In the context of Borides meant for ultra-high-temperature applications (exceeding 2500°C), Huang *et al* [48] have reported the fabrication of ZrB_2 cones using the FEF technique. McMillen *et al* [49] have demonstrated the use of AM-based Ceramic On-Demand Extrusion (CODE) technique for the fabrication of dense monolithic ZrB_2 ultra-high temperature ceramics (UHTCs) (with relative density $\sim$99%) using a mixture of oxide-carbide-nitride based ceramic powders and water-soluble organic binders (mostly Polyvinyl alcohol (PVA)). CODE has been reported as an extrusion-based AM technique for the production of complex-shaped mesoscale components [49]. However, there is hardly any report on the mechanical properties of FEF- and CODE-based ZrB_2 components to date. Feilden *et al* [50] have reported the fabrication of HfB_2 UHTC using Robocasting technique with theoretical densities of complex-shaped monolithic parts as high as $\sim$94-97% and with a bending strength of $\sim$196 $\pm$ 5 MPa at temperatures as high as $\sim$ 1950°C [50], which is comparable with the HfB_2 UHTCs fabricated using conventional techniques.

2.3 *Directed energy Deposition (DED) techniques*

The DED (also known as laser cladding) methods utilized to fabricate macroscopic ceramic parts can be classified as follows.

2.3.1 *Traditional DED (or laser cladding) techniques:*

In this technique, the printing head comprises of a nozzle for feeding ceramic powder particles to the focal point of the laser beam [51]. This is followed by the melting and solidification of the powder particles on a substrate [51].

2.3.2 *Hybrid fused deposition modelling – Directed energy deposition:*

As reported by Wang *et al* [52], this technique has been used to fabricate Ti-6Al4V-TiC composite by feeding TiC powder and Ti-6Al-4V wire into the focus of a CO_2 laser.

2.4 *Sheet lamination (Laminated Object Manufacturing (LOM)) techniques*

These processes may be classified as: (i) Traditional LOM and (ii) Computer-Aided Manufacturing of Laminated Engineering Materials (CAM-LEM).

2.4.1 *Traditional LOM technique:*

The traditional LOM technique consists of a system for deposition of green ceramic tape casted layers onto a bed for cutting the outline of each layer of the ceramic part using a CO_2 laser [22, 31]. This is followed by the passage of a heated roller over the layer for thermal activation of the binder system (of the tape) and lamination of the sheet (to the previous layer) as reported by Williams [31]. However, it needs to be mentioned that the boundary between the tapes should be untraceable after being compressed by the roller [53]. The final ceramic parts are obtained only after debinding and sintering in a furnace [22, 53].

2.4.2 *Computer-Aided Manufacturing of Laminated Engineering Materials (CAM- LEM):*

Another version of the LOM technique is the CAM-LEM method. This process has a huge similarity with that of traditional LOM, but here, instead of cutting stacked layers, each layer is cut previously and then stacked robotically for lamination (onto the working portion). The main advantage of this method as compared to traditional LOM is the formation of internal voids within each layer [31].

2.5 *Binder jetting 3D printing (BJ3DP)*

These techniques involve a selective deposition of a liquid bonding agent onto powder materials. In order to shape ceramic components, a 3DP device deposits a layer of ceramic powder and then a jetting binder material for a selective binding of the ceramic powder [22, 31]. These methods may be classified as:

2.5.1 *P-3DP (P-3DP: Powder-based three-dimensional printing) technique:*

This technique involves a sequential deposition of powder particles with a scraper or roller and subsequent printing of binder material using ink-jet printing (IJP) [31]. Using his technique, a consolidated ceramic part is obtained after burning out of the binder during sintering [31].

2.5.2 *S-3DP (Slurry based three-dimensional printing) technique:*

For the purpose of processing fine powders (< 20 μm) and improvement in sinterability of the green part, S-3DP technique tends to be much more advantageous as compared to P-3DP technique [22]. During S-3DP technique, each layer of powder bed is formed by the jetting of ceramic slurry onto a substrate. This is followed by subsequent drying of the as-cast and a selective deposition of a binder in the desired pattern [22, 31].

2.6 *Single step powder bed fusion (or SLM)*

This technique employs a laser-beam for a complete melting of ceramic powder particles. In literature [22], three different variations of powder layer deposition techniques for SLM of ceramics have been reported, namely, (i) conventional deposition (using a scraper or a counter current roller), (ii) slurry based deposition and (iii) aerosol assisted spray deposition (table 1) [22].

2.6.1 *Conventional Deposition:*

Systems for conventional deposition systems have an advantage of depositing heavy and large (typically with sizes > 5 μm) ceramic powder particles [22, 54, 55]. During this process, the gravity forces overcome the electrostatic attraction is overcome by the gravitational forces, leading to the flowing of the powder particles. Although ceramics such as pure ZrO_2, Al_2O_3 and $MgAl_2O_4$ ceramics have been processed using SLM technique, but, unfortunately micro-cracks have been observed in the manufactured ceramic parts [52]. Moreover, It has also been reported that SLM of single-phase ceramics, e.g. ZrO_2 and Al_2O_3 results in coarse grained microstructures [22, 53].

In order to reduce the extent of micro-cracking phenomenon arising due to excessively high thermal gradients, a high temperature preheating system using a CO_2 laser beam (for preheating powder layers) and a Nd:YAG laser beam (for localised melting of the ceramic powder particles), has been reported by Deckers *et al* [22]. Although using the high temperature preheating system, ceramics such as pure ZrO_2, Al_2O_3 and $MgAl_2O_4$ could be processed, however, micro-cracks were also observed in the fabricated parts. Moreover, for ZrO_2 and Al_2O_3, coarse grained microstructures were obtained [22].

2.6.2 *Slurry based deposition technique:*

SLM in combination with slurry coating as been used to produce silica-clay parts [22]. The clay used, acts as an inorganic binder for silica (SiO_2) powder during the process

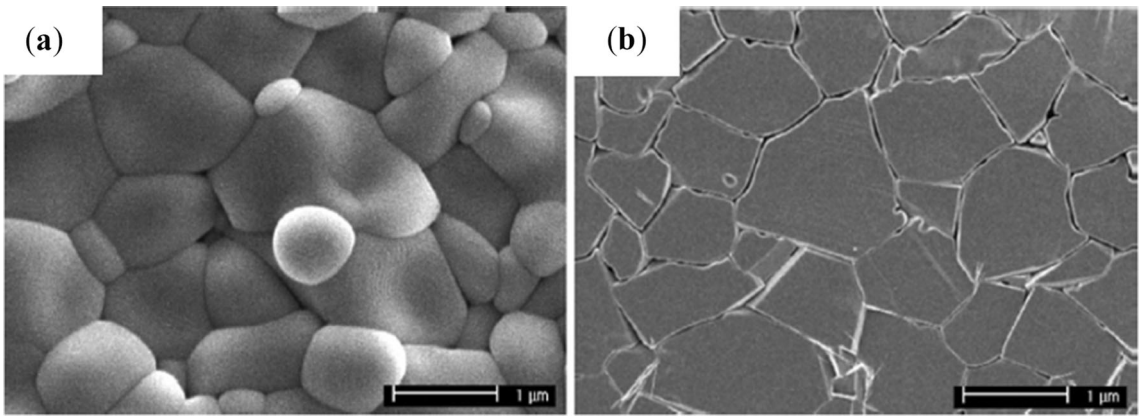

Figure 1. Scanning Electron Microscope (SEM) micrograph of the (a) surface and (b) cross-section of Al_2O_3 sample fabricated using SLM of layers deposited using aerosol assisted spray deposition technique [17].

of drying. In this way a green layer ceramic substrate is produced in order to minimise balling and provide a structural support to the ceramic part during building process. During laser scanning, the dried silica-clay layer undergoes complete melting, leading to a significant reduction of porosity in ceramic parts. However owing to the brittle nature of SiO_2 and no preheating of the deposited layers, high-energy laser scanning has been reported to easily induce thermal cracks in ceramic parts [22], rendering this process unsuitable for production of high strength parts [56–59].

2.6.3 *Aerosol assisted spray deposition:*

Preparation of powder beds for subsequent laser scanning, using this technique, was first reported by Wu *et al* [17]. This process has been reported to be useful for fabrication of single layered ceramic parts. Based on the report of Deckers *et al* [22], preparation of Alumina (Al_2O_3) suspension was performed by an addition of 5 wt.% Al_2O_3 powder to a solvent (ethanol, purity: 99.5%) with dispersant as 0.2 wt.% of polyacrylic acid (PAA). During the irradiation of the Al_2O_3 powder beds by the laser beam, the PAA has been reported to evaporate with the melting of Al_2O_3 particles (submicrometer-sized) so as to form a liquid-phase, in order to facilitate densification through liquid-phase sintering (LPS) [22]. With increasing energy density of the laser beam, an increasing extent of densification has also been reported [17, 22, 60]. Figure 1 shows a completely densified microstructure of an Al_2O_3 sample fabricated using SLM of layers deposited using aerosol assisted spray deposition technique.

2.7 *Single step powder bed fusion (partial melting)*

2.7.1 *Conventional deposition technique:*

Lakshminarayan *et al* [61, 62] have fabricated alumina (Al_2O_3)-ammonium phosphate ($(NH_4)_3PO_4$) and alumina-boron oxide ceramics using this technique. Besides, both ammonium phosphate (melting point: 190°C) and boron oxide (460°C) have also been reported to play a dual role as structural materials and binders for gluing Al_2O_3 particles [61–63].

2.7.2 *Slurry coating technique:*

In this technique, a slurry layer (powder containing) is deposited with subsequent drying. This has been reported to highly enhance the packing density of the deposited powder particles, as compared to that in case of conventionally deposited powder particles (by $\sim$ 46 vol.%) for highly loaded solid slurries [22]. Moreover, through SLS® of slurry coated layers, hydroxyapatite, Al_2O_3-SiO_2 and porcelain parts have been successfully fabricated [64–71].

2.7.3 *Slurry spraying technique:*

Klocke *et al* [72] have produced yttria stabilized zirconia (YSZ) by using direct SLS® technique. As reported [72], the process involved formation of powder layers by spraying (instead of a layer-wise deposition) ceramic suspension before drying. Moreover, cracks, observed on the SLSed layers were reported to occur by thermal contraction during cooling after irradiation using a laser beam). The amount of open porosity in the finished parts was reported to be $\sim$24–32% [72]. However, the molten powder was unable to fill all the gaps between the unmelted powder particles inspite of high packing density of the deposited green layers [72].

2.7.4 *Ring blade technique:*

This process, patented in 2004 [73] consists of a ring blade [74], also known as 'powder rack', for deposition of dry non- agglomerated submicrometer sized ceramic powder. Moreover, using this technique, it is also possible to partially melt the deposited powder particles. For the purpose of inhibit overheating of the laser scanned material, the laser is mostly applied in a

pulsed mode instead of a continuous mode [75]. Partial melting of submicrometer sized powder particles using the micro SLS® device (using Ring blade technique) has been reported to be used for the fabrication of the following ceramic parts: $A_{l2}O_3$-feldspar [74], Al_2O_3-SiO_2 [73, 75–77], feldspar [73] etc. However, the fabricated ceramic parts were reported to contain pores [22].

2.7.5 *Electrophoretic deposition (EPD) technique:*

An experimental setup for his technique as reported by Deckers *et al* [22], consists of a vertical tubular furnace for a homogeneous heating till 800°C (within a range of ± 50°C). The layer deposition process has been reported to consist of two steps. The 1st step involves deposition of a powder layer on a deposition electrode by the EPD process in an EPD cell, consisting of a positively charged Al_2O_3 suspension with a counter electrode mounted at the bottom and a deposition tool at the top of the cell. During EPD process, a DC power source is used to negatively charge deposition electrode and positively charge counter electrode. The 2nd step involves the removal of deposition tool with EPD deposited powder layer from the EPD cell and subsequent mounting into a gearbox for deposition of the powder layer in the vertical tubular furnace. Optimisation of the layer deposition and laser scanning parameters has been reported for the fabrication of Al_2O_3 ceramic parts with a high density ($\sim$ 85%) and a microstructure with average grain size $<$ 5 μm [78–82]. Although the main consolidation mechanism of this technique appears to be partial melting, but however, at present, it remains unclear as to which consolidation mechanism is active during the process. Therefore, the laser consolidation process has also been specified as direct Selective Laser Sintering®/Melting (direct SLS®/SLM) [22]. Figure 2 shows the SEM images of α-Al_2O_3 ceramic part fabricated using SLS®/SLM technique.

2.8 *Conventional deposition technique*

Solid state sintering (SSS) as consolidation mechanism during SLS® of ceramic materials at 800°C, was reported by Bertrand *et al* [83] where sintering of the preheated powder (close to the sintering onset temperature) was performed using Nd:YAG laser.

2.9 *Chemically induced binding (CIB) for single step powder bed fusion (or Selective Laser Reaction Sintering (SLRS))*

During this technique, initiate a chemical reaction occurs due to the heat of the laser beam resulting in binding of the powder particles [22, 84]. The following powder deposition systems are employed for the ceramic part fabrication through this process.

2.9.1 *Conventional deposition technique:*

Based on the report on SLS® of SiC powders in inert Ar atmosphere by Klocke *et al* [85], SiC decomposes into Si and C during laser irradiation and despite the inert nature of the Ar atmosphere, Si atoms react with O_2 to form SiO_2, which leads to the binding the SiC particles [85]. Owing to the high melting temperature of Si ($\sim$1420°C), SiC particles are also bound by molten Si [85].

2.9.2 *Slurry coating (Ceramic Laser Sintering (CLS)) technique:*

Deposition of slurry layers, consisting of aluminium phosphate and SiO_2 was first reported by Tang *et al* [86] and is based on an irreversible chemical reaction of slurry containing aluminum phosphate and silica at a temperature above 250°C.

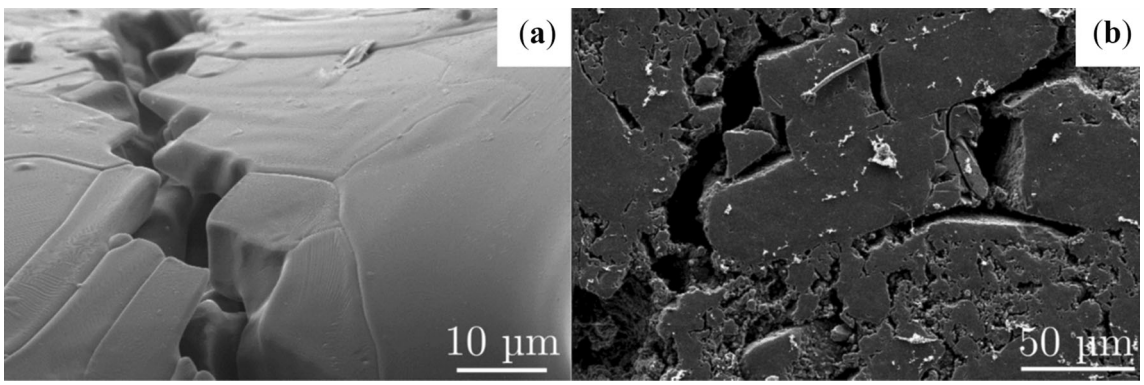

Figure 2. SEM images of α-Al_2O_3 ceramic part fabricated using SLS®/SLM technique: **(a)** unpolished scan surface with crack **(b)** polished cross-section. The image in part **(b)** has been acquired perpendicular to scan tracks [78].

Table 2. Sacrificial binders for fabrication of different ceramic parts based on a conventional SLS® system [22].

		Binder				
		Inorganic	Organic			
			Acid	Wax	Thermoset	Thermoplast
Ceramic	Al_2O_3		Stearic acid	Carnauba wax		Nylon-12, polypropylene, polystyrene, PMMA
	Al_2O_3-B_2O_3	HBO_2				
	Al_2O_3-glass-B_2O_3	HBO_2				
	Al_2O_3-ZrO_2-TiC			unspecified		PMMA
	Apatite-mullite					Unspecified acrylic binder
	Graphite				phenolic resin	Nylon 11
	K_2O-Al_2O_3-SiO_2				epoxy resin	
	SiO_2				unspecified	
	SiC				phenolic resin	
	ZrO_2				unspecified	Polypropylene
	ZrB_2		Stearic acid			

2.9.3 *Ring blade technique:*
This technique was first used to fabricate Si-SiC parts through SLS® of SiC [22] using an Nd:YAG laser (wavelength ∼ 1064 nm) in a continuous mode (in order to decompose a fraction of the irradiated SiC powder particles). This yielded Si (in elementary form), which became the bridging material for unreacted SiC grains [73, 76–79].

2.9.4 *Conventional deposition system:*
This is a method for fabrication of ceramic parts (for elevated temperature applications) by low temperature selective laser sintering (SLS®) of ceramic particles and a binder material (sacrificial in nature) [87]. The binder melts and hence binds the ceramic particles together. Using this process, a ceramic part is obtained after debinding in a furnace, as shown in table 2 [22].

Indirect SLS® with the use of a sacrificial binder phase aids in the fabrication of crack free ceramic parts, but however, there is a compromise on the final density, i.e. the density of the part after debinding and before sintering has been reported to be generally low (limited to only ∼ 39-80%) [22, 88, 89] which has been attributed to the occurrence of voids powder particles (size: 10-100 μm) [22], after SLS®. Moreover, these voids have been reported not to disappear during debinding and Solid State Sintering (SSS) and hence, are present in the finished part [88–92]. In order to reduce the number of voids (primarily, inter-agglomerate in nature), Shahzad [93] and Deckers [94] have reported: (i) laser re-melting (multiple irradiation of powder layers), (ii) cold, quasi and warm isostatic pressing of the parts (produced by SLS®) and (iii) infiltration of parts obtained during different stages of the partial melting process. Moreover, Indirect SLS® (through partial melting of composite agglomerates) has not only been used to produce pure ceramics, but also composites [95–100]. For instance, Gill *et al* [96] have reported SLS® of SiC-PA ceramic-polymer composites. Evans *et al* [100] have reported that infiltration of SiC preforms with molten Si produces SiC-Si cermets. Stucker *et al* [97, 98] have used the SLS® technique to manufacture ZrB_2 green parts (with a density of ∼31% in pre-infiltrated condition) followed by debinding, sintering, and infiltration (with Cu) for applications in Electrode Discharge Machining (EDM) electrodes. In addition, a previous investigation on ZrB_2 by Sun and Gupta [99] has reported that fine ZrB_2 powders produced by the SLS® technique have enhanced surface wettability and sinterability. Leu *et al* [91, 92] have fabricated ZrB_2 flexural test bars and 3D fuel injection components (for application in spacecraft) (using SLS) with ∼80% density and flexural strength ∼195 MPa.

2.9.5 *Multi-step powder bed fusion by Ceramic Laser Gelling (CLG):*
This process works on the principle of initiation of physical or chemical gelling of a colloidal suspension (a sol) by the

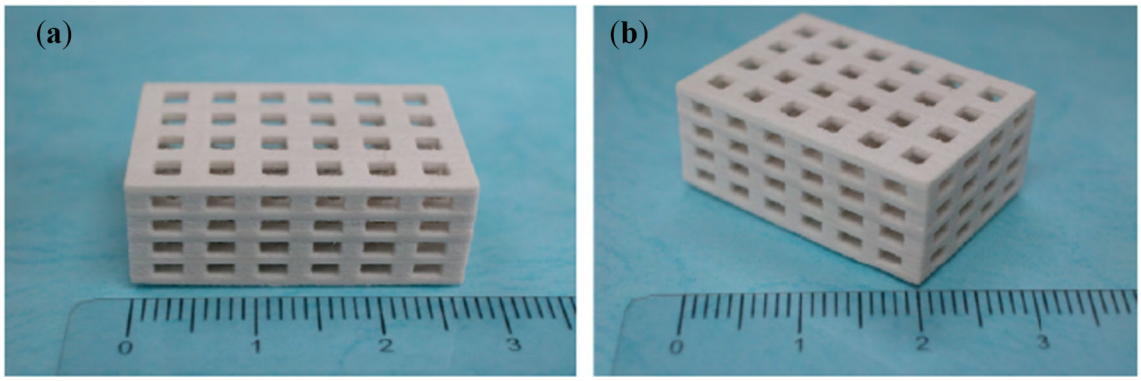

Figure 3. A silica part with inner channel structure fabricated using CLG technique. Parts **(a)** and **(b)** show the image of the same part with different views [102].

induction of heat energy through a laser beam, leading to an increase in viscosity of the sol (once gelled) and subsequent development of rigidity through formation of crosslinked 3D network [22]. For instance, during deposition of a thin film using a slurry coater, CO_2 laser irradiation can be utilised for the purpose of drying a portion of the deposited layer, in order to form a physically gelled network of solid particles. The portion of slurry film, left unscanned by the laser beam, remains as a slurry [22, 100]. Yen *et al* [101] have used slurry comprising mainly of Al_2O_3 powder, SiO_2 sol and deionized (DI) water, in order to fabricate Al_2O_3 - SiO_2 components. Liu *et al* [102, 103] have reported that using CLG technique, a pure SiO_2 part (figure 3) can be obtained by mixing SiO_2 sol with SiO_2 powder.

2.9.6 *Vat photopolymerization techniques:*

These techniques (based on stereolithography (SLA) and also termed as Ceramic Stereolithography (CerSLA [22], CSL [22]) and sometimes, even termed as Lithography based Ceramic Manufacturing (LCM [22])) involve a selective curing of a liquid photopolymer using light-activated polymerisation [1]. During SLA, a UV radiation is typically used to scan ceramic powder containing slurry layers, leading to chemical gelling of these layers. The final ceramic part is obtained after debinding the resulting polymer and sintering the material obtained after debinding [22]. Moreover, based on the sizes of the final ceramic parts produced these techniques can be classified into two types, namely, (i) Macro SLA and (ii) Micro SLA.

2.9.6.1. Macro SLA technique:

In the context of macro SLA technique, Griffith *et al* [104] and Halloran *et al* [105] have suggested the replacement of laser source by Light Emitting Diodes (LEDs) or even halogen lamps while transferring the desired pattern on the photocuring liquid and coined this technology as Large Area Maskless Photopolymerization (LAMP). As reported by Deckers *et al* [22], during LAMP, each layer undergoes a rapid patterning through UV exposure in the form of a bitmap defined using a light modulator. Moreover, it is also possible to use a medium consisting of UV curable resin (acing as an organic binder) and methanol (acting as both solvent and dispersant), resulting in shrinkage of the deposited slurry volume [106]. Besides, another route to produce the UV curable resin was devised by De Hazan *et al* [107], in which, adsorption of the surfactants was carried out in an aqueous media under controlled pH conditions on Al_2O_3/ZnO powder particles. The extent of photopolymerisation can be described using the equation developed by Jacobs [108], based on Beer-Lambert's Law. Figures 4 (a-d) show fabrication process of ZrO_2 toughened Al_2O_3 (ZTA) ceramic gear using SLA technique.

2.9.6.2. Micro SLA technique:

This technique is more or less similar to that of macro SLA technique, but with the only exception that this technique has the capability to produce complex shaped 3D components with length scales less than even 1 mm, as reported by Bertsch *et al* [110].

3. Alternative AM methods for fabrication of ceramic parts (highlighted in table 1)

3.1 *Electrophoretic deposition (EPD) technique*

This technique involves electrophoresis (migration of charged colloidal particles in a liquid medium) and a controlled deposition of these particles to shape a 3D component using an electric field between electrodes [111].

3.2 *Electro photographic printing (EP) technique*

In this method, as described by Deckers *et al* [22], a photoreceptor plate, containing an electrostatic image of a layer belonging to the ceramic part (to be manufactured), is aligned over a powder bed. Due to the electrostatic charge, the ceramic powder particles get attracted towards the

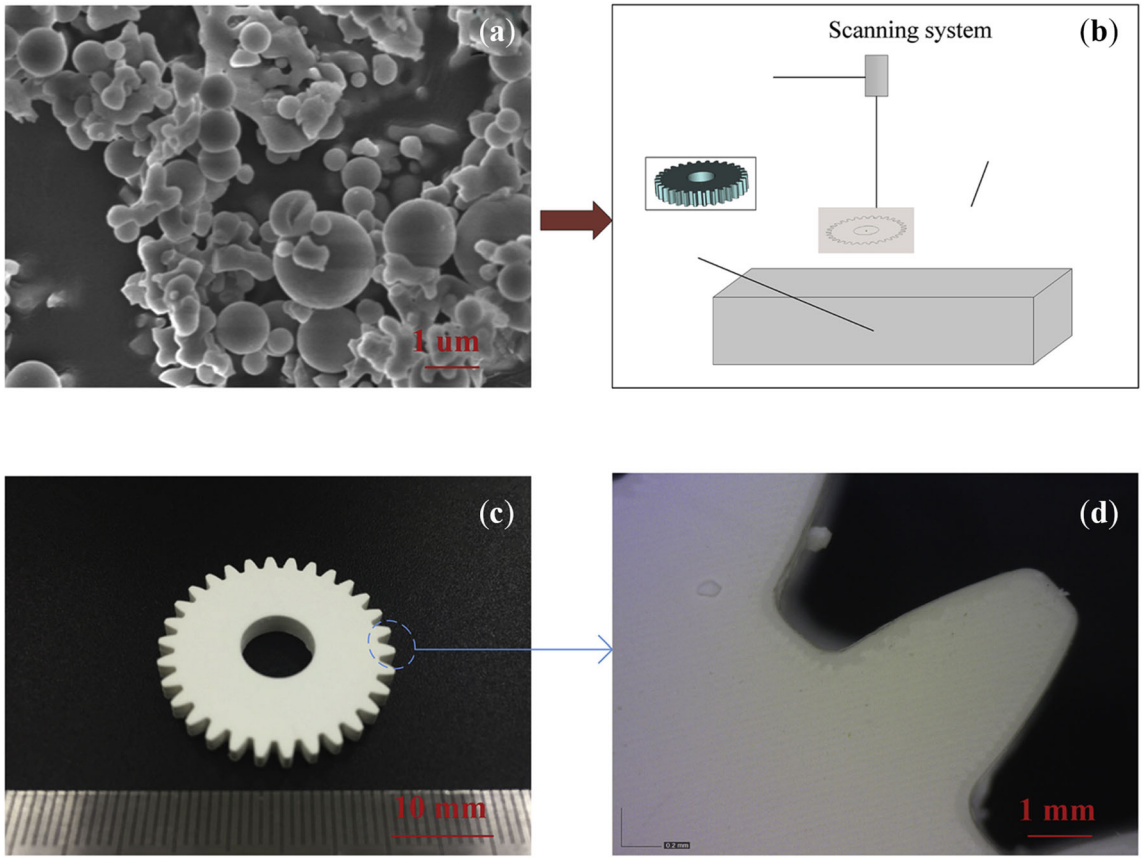

Figure 4. Schematic showing the fabrication process of ZrO_2 toughened Al_2O_3 (ZTA) ceramic components using SLA technique: **(a)** ZrO_2/ Al_2O_3 powders for preparing paste, **(b)** 3D printing of ceramic parts using SLA, **(c)** Sintered Al_2O_3 /ZrO_2 ceramic gear and **(d)** its microstructure [109].

photoreceptor plate in the exact shape of the layer (or sometimes, in the negative shape of the layer if printing of support material is required). After a sequential charging and deposition of powder layers, the printed layers are made to undergo compaction and final sintering for producing the ceramic part.

4. Fabricating cermets through additive manufacturing

On the basis of feedstock, AM processes are classified into three categories: namely, powder-based, liquid-based, and solid-based techniques [112, 114]. At present, selective laser sintering/melting (SLS®/SLM), binder jet (3D printing (3DP)), laser engineering net shaping (LENS), direct laser deposition (DLD) and more recently, robocasting [114–119] are processes commonly used for the fabrication of cermets. Figure 5 shows cermet parts fabricated by three common AM processes.

4.1 *Selective Laser Melting (SLM)*

Khmyrov *et al* [120, 121] have investigated the phase evolution during fabrication of WC with variation in wt.% Co using SLM and reported a complete dissolution of WC in all samples except for the sample containing 6 wt.% Co and also attributed the dissolution of WC with the formation of different carbides to the reduction in carbon content of SLM samples.

Moreover, for producing crack-free WC-Co samples, two compositions with 75 wt.% and 50 wt.% Co were used [120]. For a uniform distribution in the powder particles, the powder mixture was milled for 2 h at 200 rpm. Fabrication of SLM samples was carried out using a hatching distance of 100 µm (Power: 50 W, scan speed: 100 mm/min) [120]. The sample with 75 % Co was reported to be crack free (figure 4). The formation of brittle W_3Co_3C phase was reported to be the main reason for the formation of cracks in samples with 50 wt.% Co [120]. Moreover, a correlation of the hardness of metal-ceramic composites with the size of the carbide particles after SLM has also

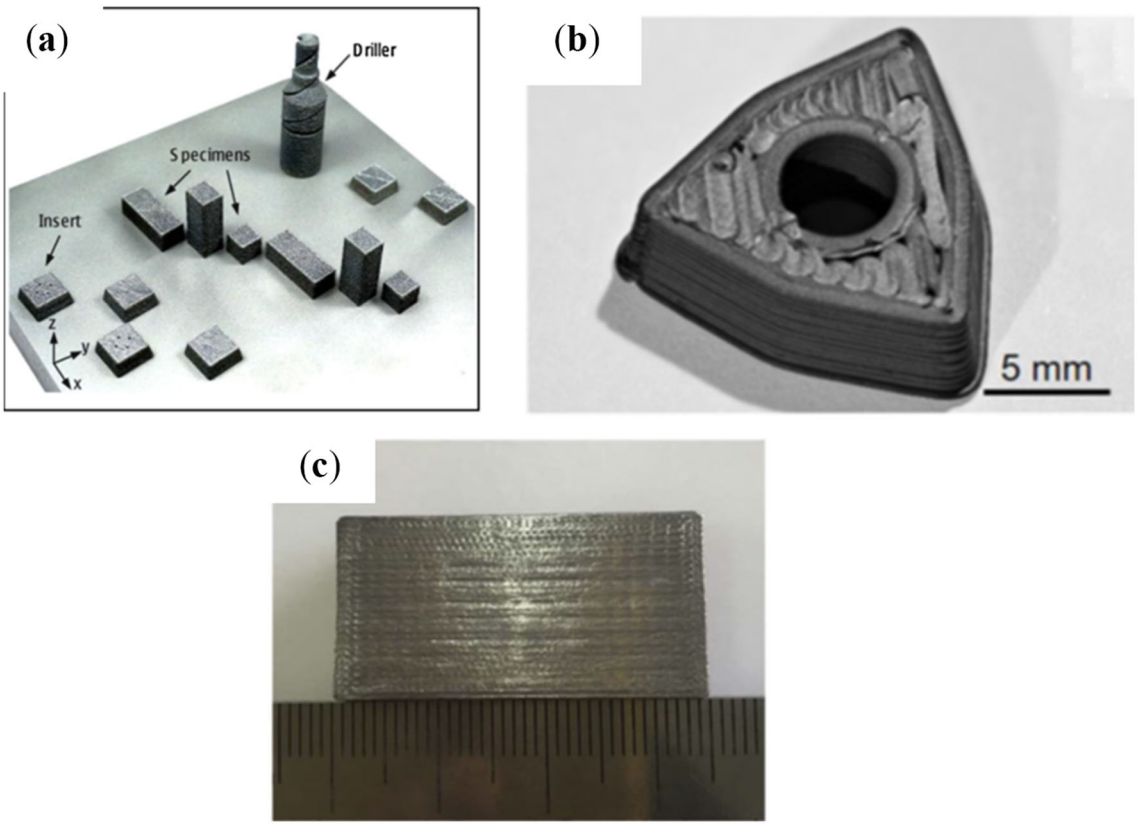

Figure 5. **(a)** Cermet parts fabricated using SLM [113], **(b)** Fused Filament Fabrication (FFF) [117] and **(c)** Extrusion-Based 3DP [118].

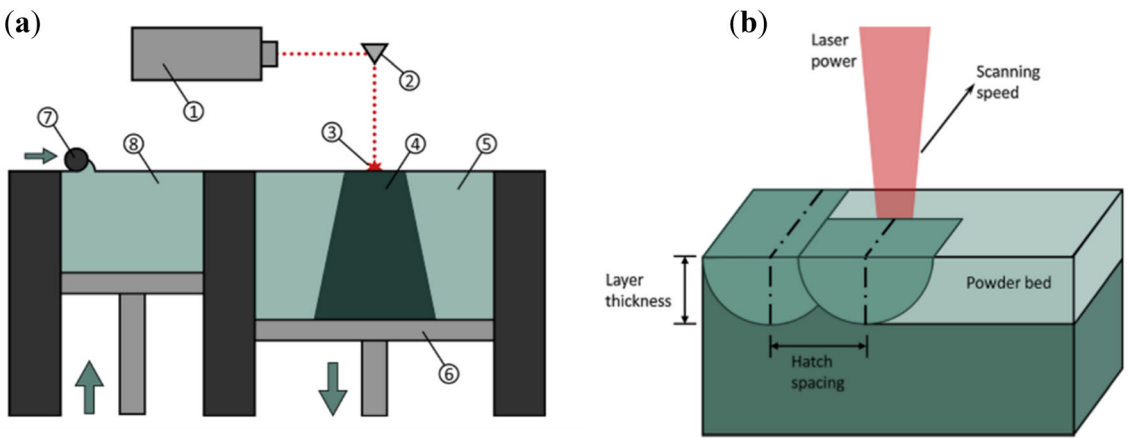

Figure 6. **(a)** Schematic of SLS®/SLM process: (1) laser, (2) scanner system, (3) molten pool, (4) printed object, (5) powder bed, (6) build platform, (7) powder roller, and (8) new powder stock. **(b)** Schematic representation of parameters (exposure parameters) influencing volumetric energy density (EV) during SLM [112].

been reported [120, 121]. Figure 6(a) shows a schematic of SLS®/SLM process and figure 6(b) represents exposure parameters influencing volumetric energy density (EV) during SLM technique.

Grigoriev *et al* [122] and Campanelli *et al* [123] have reported that formation of cracks in the manufactured specimens with WC (brittle phase) content occurs due to a significant difference in the melting points and

coefficient of thermal expansion between WC and binder. Domashenkov *et al* [124] have investigated the microstructural evolution and mechanical response of WC-12% Co samples produced by SLM process using (i) conventional powder particles and (ii) nanophase powder particles and reported that formation of W_2C and W_2Co_4C occurs due to decarburization of WC during melting and solidification. Based on the experimental observations [124], two regions containing coarse and fine carbides were observed and hardness values were reported to depend on the size of carbides in samples fabricated using conventional and nanophase powder particles. Higher hardness values were reported for finer carbides (table 3).

4.2 *Selective Laser Sintering (SLS®)*

Gu and Shen [125] have investigated the microstructure and mechanical properties of laser sintered WC-Co/Cu nanocomposites using X-ray Diffraction (XRD), Atomic Force Microscopy (AFM), Scanning Electron Microscopy (SEM) and Energy Dispersive Spectroscopy (EDS). Based on this work [125], a double stage wetting mechanism during laser sintering of WC-Co/Cu nanocomposites was proposed (figure 7). From figure 7, it may be observed that at the initial stages of wetting, Co forms a homogeneous coating on WC particles (figures 7(a and b)). However, once temperature exceeds melting point of the matrix (Cu [125]), there is formation of a sintering (melt) pool leading to Maragoni convection [108]. Maragoni convection, formed as a result of the large temperature gradient between the edge and centre of the melt pool due to Gaussian laser beam, leads to wetting of WC-Co with liquid Cu (2^{nd} stage of wetting) (figure 7(c)). The two-stage wetting mechanism of WC leads to a homogeneous distribution of WC phase in a metal matrix (Cu [125]) (figure 7(d)).

Kumar [126] have investigated the influence of isothermal heat treatment (at 400, 600, 800 and 1000°C for 3h) on the hardness and wear behaviour of the fabricated specimens and reported that diffusion of the elements leading to the homogenization and formation of the eta phases: M_6C and $M_{12}C$ during heat treatment, leads to improvement in mechanical properties [112]. Gu and Meiners [127] have reported hardness fluctuations in the longitudinal section of WC-10 %Co cermet as a result of inhomogeneous distribution of WC particles (figures 8(a-c)). Gu *et al* [128] have reported an increase in the microhardness of SLS samples with the addition of a rare earth oxide (La_2O_3) to WC-Co/Cu powder (weight ratio: 50(WC-Co):49Cu:La_2O_3). Moreover, from figures 8(d-k), it may be inferred that the morphology of M6C carbides is largely dependent on laser scan speed during SLM [127].

4.3 *Laser engineered net shaping (LENS)*

This technique has been widely used for fabricating cermet components in addition to being a surface treatment technique [112]. Based on an extensive review on AM of cermets by Aramiana *et al* [112], the effective process parameters influencing the microstructural evolution during the LENS process are: (i) laser power, (ii) powder feed rate, (iii) traverse speed of the laser beam, and (iv) working distance. For example, in order to obtain large layer thickness, the laser power or powder feed rate may be increased, or the traverse speed of the laser beam may be decreased. Short working distance has been reported to lead enhance microstructural uniformity and a slight increase in density of the final product [128, 129].

Xiong *et al* [129] have reported that on the basis of position along the height of the samples (during LENS process), mechanical properties may be varied due to change in the cooling rate along the height of the specimen of WC-10 % Co cermets (with lower hardness values reported at layers close to the top surface). Moreover, it has been stated optimisation of process parameters during LENS is necessary for the production of dense and crack-free thin wall specimens [129]. Sahasrabudhe and Bandyopadhyay [130] have reported AM of reactive in-situ ZrB_2-based UHTCMCs in Zr metal matrix using the LENS technique. It has been reported that a proper bonding was achieved between Zr metal (in α-phase) and Zr-BN composites with Ti-6Al-4V (α-β Ti alloy) substrate [130]. In this context, LENS processing of the mixture of Zr and Zr-BN powders has been reported to lead to β phase of Zr [130]. Vickers microhardness of pure Zr was measured to be $\sim 280 \pm 12$ HV and was reported to increase with increasing BN content [130]. For instance, Vickers microhardness for Zr-10% BN was reported to be $\sim 562 \pm 10$ HV [130]. In addition, it has also been highlighted that Zr-BN composites cannot be fabricated using conventional fabrication techniques, which are currently used in the field of UHTCMCs [130].

High magnification SEM-BSE image of the sample shown in figure 9 shows that the boundary between two deposited layers consists of fine (< 100 nm) particles of WC in the darker region and large WC particles (submicron scale) on the brighter side, formed as a result of grain growth in the binder [131–134]. Moreover, from figures 10(a and b), it may be inferred that the low intensity of laser beam coupled with short working distance (for the laser), leads to a uniform microstructure without layer boundaries.

4.4 *Direct laser fabrication (DLF) technique*

DLF has been reported to be a promising method for a layer-by-layer deposition of complex 3D samples with a direct deposition of powders in the melt pool [114]. In-situ

Table 3. Microhardness obtained from nano phase and conventional WC/12Co [124].

Micro hardness ($HV_{0.5}$)	Coarse zone (nano phase sample)	Fine zone (Nano phase sample)	Coarse zone (Standard sample)	Fine zone (Standard sample)
Average	1496	1542	1384	1515
Minimum	1400	1429	1053	1153
Maximum	1588	1697	1588	1660

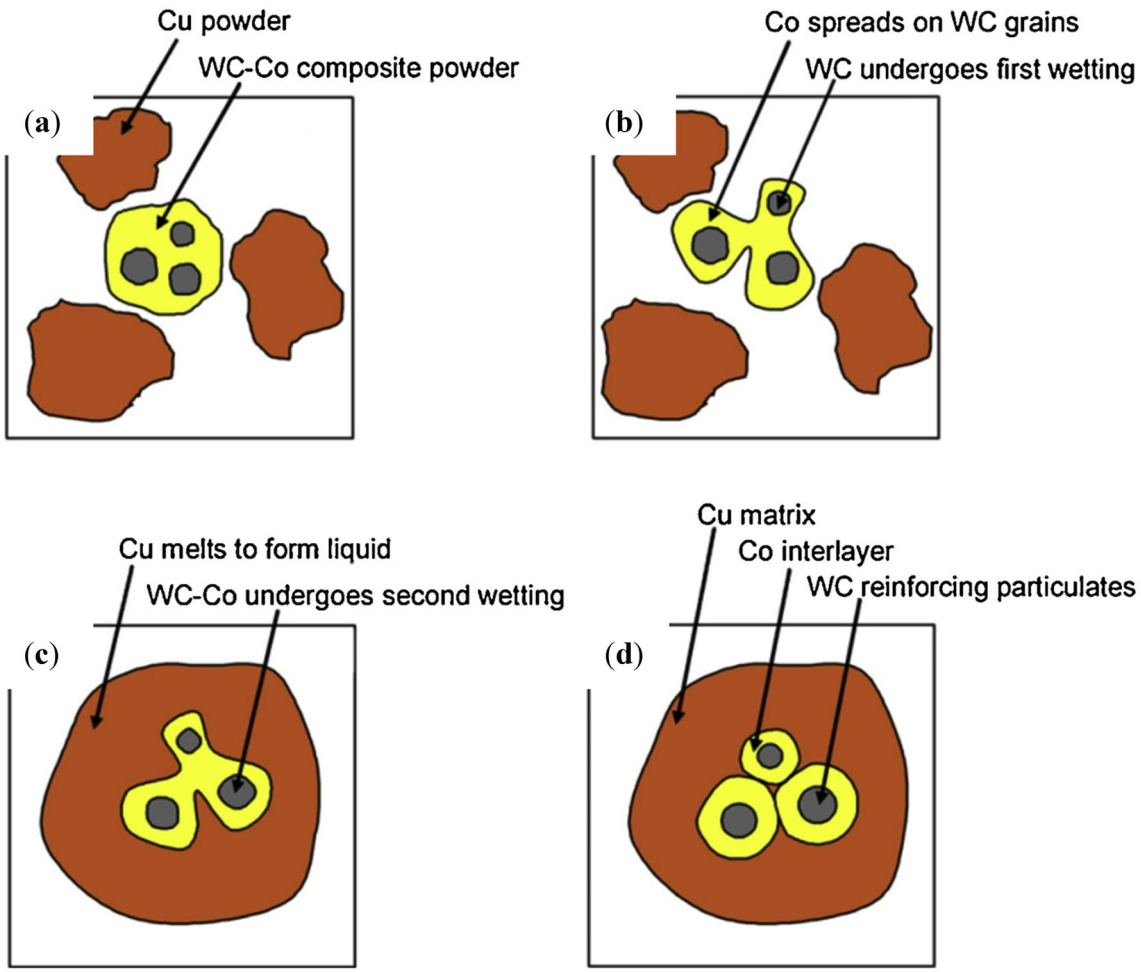

Figure 7. Schematics **(a-d)** illustrating double stage wetting mechanism during direct laser sintering (DLS) of WC-Co/Cu composite [125].

fabrication of TiC-(20, 30, 40 vol.%) Ni cermet by direct laser fabrication (DLF) has been reported [136]. Moreover, it has also been reported that the bending strength and hardness of the TiC samples (fabricated using DLF technique) decrease due to reduction in the volume fraction of ceramic phase with increasing Ni content in the binder. However, the influence of Ni (present in binder phase) on the above mechanical properties of TiC-(x vol.%) Ni cermet still remains unaddressed.

4.5 *Binder jet 3D printing (BJ3DP) technique*

This is another technique that has been used for the fabrication of WC-12 %Co cermet [134–136]. Enneti *et al* [116] have reported the wear behaviour of WC-12% Co cermet fabricated using BJ3DP technique. Binder jet 3D printed cermet has been reported to exhibit a lower loss of volume in comparison to the conventionally fabricated cemented carbides [137, 138]. Moreover, the enhancement in wear

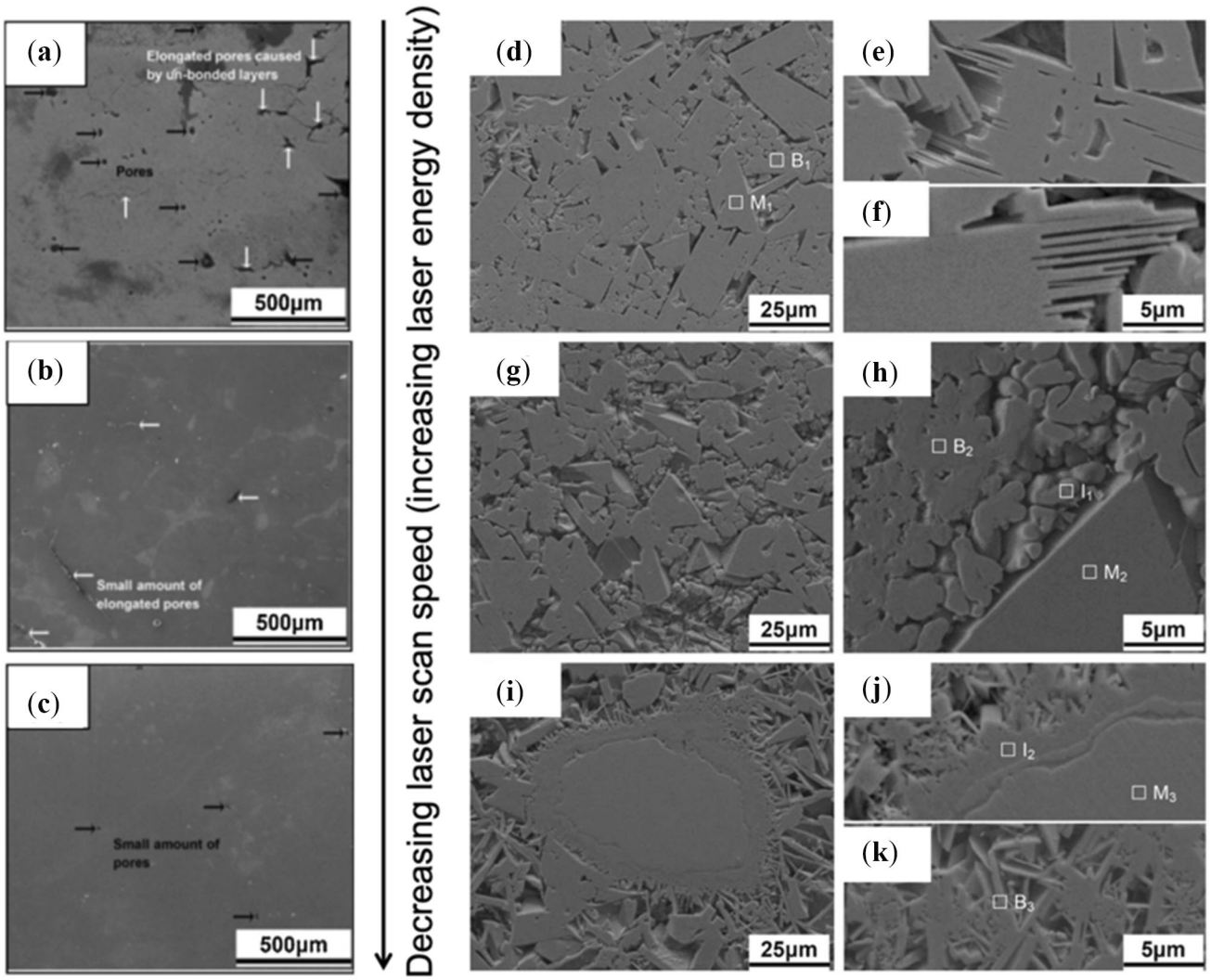

Figure 8. Cross-sectional SEM micrographs of SLM-based samples at **(a, i-k)** 1.2 m/s, **(b, g, h)** 1.0 m/s, **(c, d-f)** 0.8 m/s scan speeds of the laser. For part **(d),** M_1: Ceramic Matrix and B_1: Metallic binder. For part **(h),** M_2: Ceramic Matrix, B_2: Metallic binder and I_1: Granular precipitates at interface. For parts **(j and k),** M_3: Ceramic Matrix, B_3: Metallic binder and I_2: Ring-shaped interfacial layer [127].

resistance of WC has been attributed to a dual grain-sized microstructure in the BJ3DP material (after sintering, figure 11).

Post infiltration of BJ3DP components with a molten metal can be used for fabricating cemented carbides [112]. A number of investigations in this direction have reported that by using this approach, fully densified cermet parts with high hardness and fracture toughness comparable with that of conventional cermets can be attained. However, even with this technique, some of the major AM challenges including cracks, shrinkage and porosities remain unavoidable [137–140].

4.6 *Extrusion-based 3D Printing technique*

In this technique the feedstock can be a wire or granulated powder particles which are known as fused-filament fabrication (FFF) and composite-extrusion modeling (CEM), respectively. In both techniques, the feedstock is in fused state [112]. Lengauer *et al* [117] and Michael *et al* [141] have reported the fabrication of (Ti(C,N), WC,(Ta,Nb)C, Cr_3C_2)-Co, Ni cermet by FFF method and WC-Co by CEM process. Although, the microstructure obtained was reported to have a high level of similarity to that of conventionally fabricated parts, however, the full density could not be attained. Besides, the surface topography was reported to

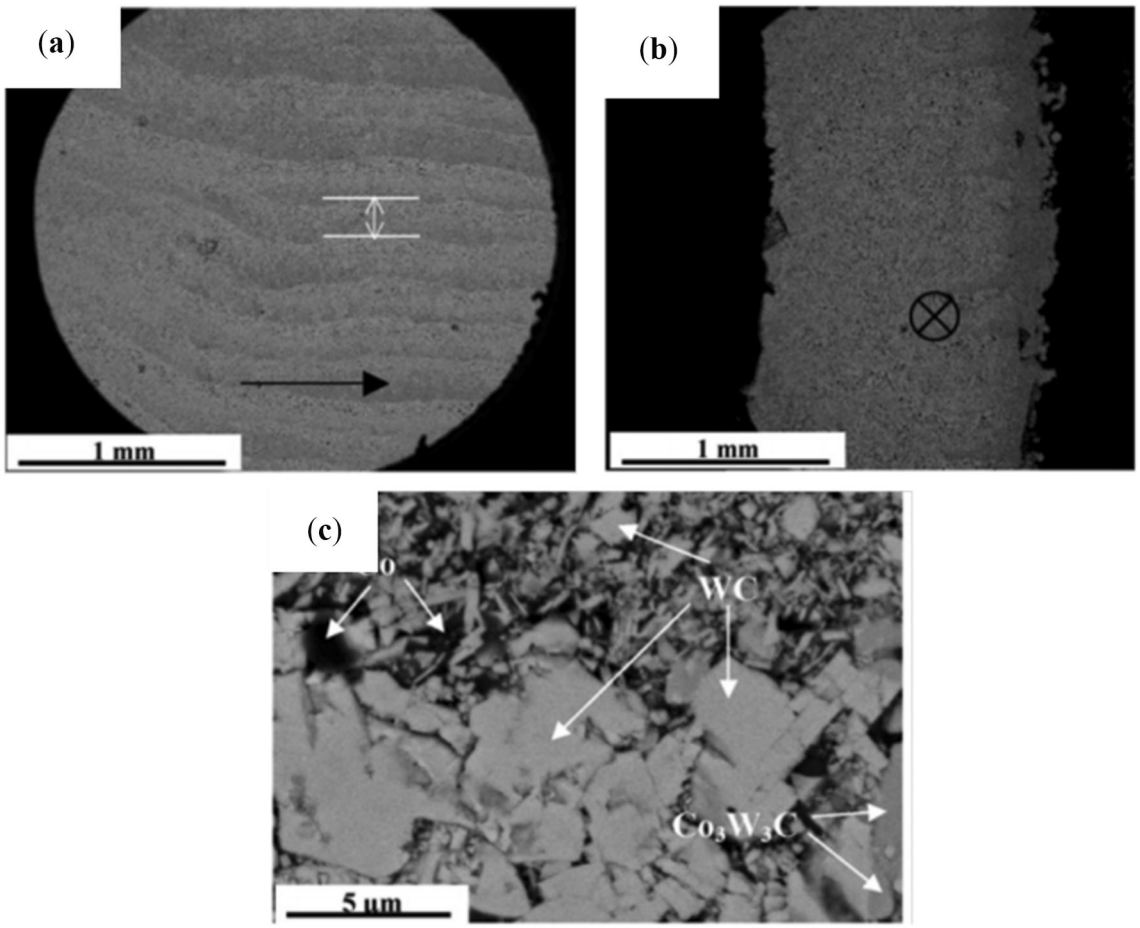

Figure 9. SEM-BSE images of a LENS WC–Co thin walled specimen fabricated using a laser beam (power: 200 W): **(a)** side view image of the alternate layers; **(b)** cross-sectional view (the circle with a cross shows the direction of deposition, normal to the section); **(c)** SEM micrograph (at higher magnification) of **(a)** showing details of the boundary region between the sintered layers [131].

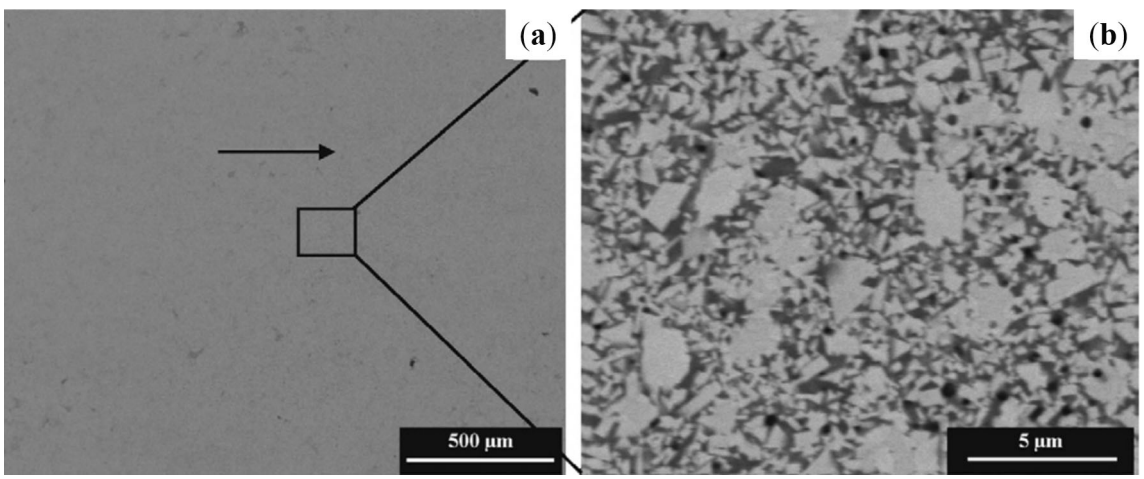

Figure 10. SEM-BSE images of WC-10 wt.% Co sample at **(a)** low magnification and **(b)** High magnification. The black arrow in part **(a)** represents deposition direction. Part **(b)** shows fine WC particles [131].

be rough with a high level of porosity between the deposited layers. These were attributed to the lack of process parameter optimisation [112].

4.7 *3D Gel Printing (3DGP) technique*

Zhang *et al* [118] have reported the fabrication of cermets (density: 99.93 %) through solid loading by 3DGP. Moreover, it was reported that the lower the extent of solid loading, the higher is the amount of solvent and organic binder in 3DGP samples [118]. The high content of both the solvent and organic binder has been reported to lead to the formation of a high level of porosity in samples during debinding and sintering [118]. Increasing the extent of solid loading has been reported to improve the hardness and transverse rupture strength of sintered 3DGP specimens [118]. However, surface treatment methods (such as polishing and finishing) are necessitated to fulfill the requirements of the part for real-life applications [112].

Table 4 summarises the starting materials and working principles of different AM-based techniques. But, table 5 shows the power source along with strengths and weaknesses of different AM techniques for the fabrication of ceramics and cermets.

5. Future perspectives and outlooks

5.1 *From the viewpoint of fabrication techniques*

It appears that there currently exist a number of limitations on the practical applications of AM based ceramics, which mainly includes the lack of microstructural quality control with the fabricated ceramic and cermet parts. Besides, a number of defects, particularly ranging from 2-D (surface) defects (such as grain boundaries, interphase boundaries, etc.) to various 3D (volume) defects (mainly, porosity) are associated with AM based ceramic and cermet parts [147, 148], which require extensive microstructural investigations to be overcome. Moreover, the intrinsic staircase effect associated with AM techniques leads to notch sensitivity issues of final ceramic and even cermet parts [147]. Besides, the need for post-processing techniques (debinding and sintering), as discussed in the previous sections, signifies that a lot of challenges associated with complex geometry designs for traditional ceramic and cermet manufacturing are also applicable for ceramics and cermets fabricated using AM based techniques, which primarily include the limitation of thickness of the final part and distortion associated with debinding/sintering.

In the context of indirect (multi-step) AM processes, making use of a binder material, the time-consuming debinding (binder removal) step, renders these processes as unsuitable for a rapid production of ceramics. Although direct (single step) AM processes (Powder bed fusion and Directed energy deposition) do not have this limitation, but however suffer from non-versatility, in terms of producing ceramic parts, unlike that of indirect AM processes [22].

Moreover, during powder bed AM approach, ceramic powder particles tend to exhibit lower flowability [144]. On the other hand, the major problem associated with powder suspension feedstock based AM techniques is the limitation in terms of the content of the ceramic solid, limiting the maximum achievable density of the finished ceramic parts and hence, necessitating optimisation of different process parameters in sintering strategies such as liquid phase sintering (LPS) and Hot Isostatic Pressing (HIP) [145, 146].

Although, a number of reviews on AM of ceramics and cermets have mentioned about the key factors required for the fabrication of the ceramic pastes during extrusion based shaping processes [144, 146], however the flow of viscous ceramic pastes needs be modeled, in order to prevent cracking in final parts [145]. Moreover, a textured microstructure may be obtained due to flow-induced alignment of ceramic particles during material extrusion processes [145], necessitating the viscous ceramic paste to be free of large aggregates. In addition, during debinding of green ceramic parts made of powder injection molding (PIM), broad temperature range of binder decomposition leading to an easy escape of the evaporated gas phase from the binder has been reported to minimise the extent of cracking in the debinded parts [118, 144]. In this regard, slow decomposition of the binder has also been reported to be beneficial for retention of the final part shape [145]. However, the development of new binder and slurry systems for AM based ceramics and cermets is an avenue which is presently unexplored and offers huge potential for future investigations.

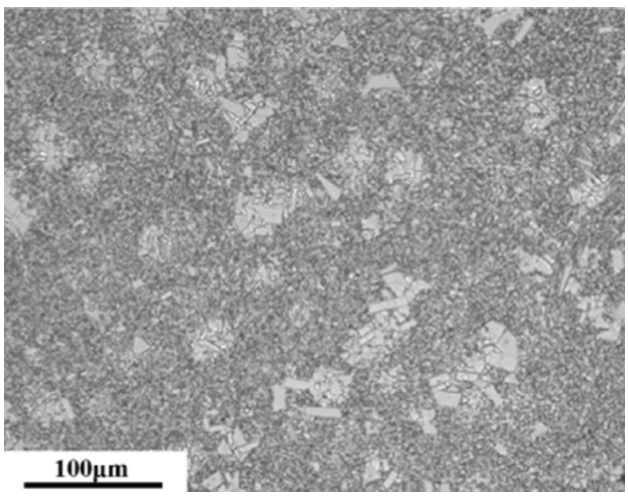

Figure 11. Dual grain sized microstructure (after sintering) of WC-12 %Co [116].

Table 4. Starting materials and working principles of different AM-based techniques [142].

State of starting material	Process	Working principle	Phase change
Liquid	SLA	Laser scanning/light projection	Photo polymerisation
Filament/Paste	FDM	Continuous extrusion	Solidification by cooling
	Robocasting		-
	FEF		Solidification by freezing
Powder	SLS	Laser scanning	Partial melting
	SLM	Laser scanning	Compete melting
	EBM	Electron beam scanning	Complete melting
	3DP	Drop-on-demand binder printing	-
Solid sheet	LOM	Feeding and binding of sheets with additives	-

Table 5. Power source, strengths and weaknesses of different AM techniques [143–147].

Category	Technique	Power source	Strength and weakness
Material Extrusion	Fused Deposition Modeling (FDM)	Thermal Energy	Strength: Inexpensive Multi-material printing Weakness: Limited part resolution
	Contour Crafting		Poor surface finish
Powder Bed Fusion	Selective Laser Sintering (SLS)	High-power Laser Beam	Strength: High design accuracy Fully dense parts
	Direct Metal Laser Sintering (DMLS)		High specific strength and stiffness Weakness:
	Selective Laser Melting (SLM)		Repeated powder recycling required.
	Electron Beam Melting (EBM)	Electron Beam	Support and anchor structure required.
Vat Photopolymerisation	Stereolithography (SLA)	Ultra-violet laser	Strength: High building speed Good part resolution Weakness: Leads to Overcuring, scanned line shape Not economical
Material Jetting	Polyjet/Inkjet Printing	Thermal Energy/ Photocuring	Strength: Multi-material printing Good surface finish Weakness: Low-strength material
Binder Jetting	Indiect Inkjet Printing (Indirect 3DP)	Thermal Energy	Strength: Full colour object printing Wide range of materials may be fabricated Weakness: Requires infiltration during post-processing Highly porous finished parts.
Sheet Lamination	Laminated Object Manufacturing (LOM)	Laser Beam	Strength: High surface finish Highly economical Weakness: Material cubing issues
Directed Energy Deposition	Laser Engineered net Shaping (LENS) Electronic Beam Welding (EBW)	Laser Beam	Strength: Repair of damaged parts Functionally-graded Material printing Weakness: Requires extensive post-processing

5.2 *From the viewpoint of fundamental research*

Although there have been a number of investigations aimed at optimisation of different processing parameters in AM based manufacturing of ceramics and cermets [1–24], however, there still remains a limited understanding on the influence of different processing parameters on the microstructural evolution which is critical to address the major challenges, particularly, (i) low density and (ii) poor mechanical properties which act as major obstacles to a large scale application of these materials in different sectors, such as defence, aerospace, electronics, healthcare etc. Poor mechanical properties in AM-based ceramics and cermet components primarily arise due to microstructural heterogeneities [22]. The microstructural heterogeneities mainly arise due to non-equilibrium processing involved in AM-based techniques [22] . Recently, Liu *et al* [147] have reported the microstructural evolution of $Al_2O_3/GdAlO_3/ZrO_2$ ternary eutectic ceramics using the SLM technique. It has been reported that there is a transition from "Chinese-script" to lamellar and to rod-like eutectic structure and from lamellar to rod-like eutectic structure in a single melt pool due to variations in eutectic growth behavior and volume fraction of constituent phases (figure 12) [147]. The evolution of the "Chinese-script" morphology of the ternary eutectic has been attributed to a high undercooling and solidification rate associated with SLM [147].

Moreover, an increase in the solidification rate (from the surface to the bottom of the melt pool) has been reported to decrease interphase spacing and an increase in Vickers microhardness and fracture toughness. This has been attributed to extensive crack propagation at the top of the melt pool and cracks bridging and arrest at $Al_2O_3/GdAlO_3$ (GAP) eutectic phase at the bottom of the melt pool. As shown in figures 13(a-d), there is no apparent cracking or porosity on the surface or in the interior of the sample other than the quenching zone [147]. Besides, figures 13(b and c) show a well-developed bond between the substrate and the solidified layer. The absence of cracks in the $Al_2O_3/GdAlO_3/ZrO_2$ ceramic has been attributed to sufficient energy input by the laser, spherical powders, and high-temperature preheating in an oxygen-free atmosphere. Figure 13(b) also shows that the solid-liquid interface shows a non-planar shape at the macroscopic level, leading to a modification in the eutectic morphology of GAP. Based on Triantafyllidis' Model [151], pores are formed due to the trapping of air bubbles at the solidification interface front in the quenching zone. High cooling rates caused an abrupt turning off of the laser beam leads to higher solidification interface velocity than bubble velocity, as shown in figures 13 (a-d). Figure 14 shows the microstructural evolution at different distances along with the melt pool. Figure 15 illustrates the microstructural features along the edge and vertical center direction of the melt pool (as marked in figures 13(b and c)). It is observed that there is a parallel growth of the microstructure perpendicular to the melt pool boundary (figures 15(a-c)). As shown in figures 15(d-f), there is a decrease in the angle between the growth direction and laser scanning direction from the bottom to the top of the melt pool. Similar observations have also been reported by Cao *et al* [149] and Larrea *et al* [150].

Guessasma *et al* [151, 152] have reported that the discontinuity associated with layer-by-layer deposition technique in AM gives rise to a number of limitations in AM components such as mechanical anisotropy, poor interfacial cohesion between deposited layers, and porous microstructures. All the aforementioned limitations promote cracking between deposited layers and hence, degrade the overall mechanical performance of the AM components [155]. More particularly, during tensile deformation, the pores act as sites of local stress concentration leading to the initiation of micro-cracks [152]. Most of the engineering applications dealing with ceramics and cermets utilize their high compressive strengths. Under compressive loads, although porosities may undergo closure, however, lateral expansion may lead to shear-induced failure of the AM-based components [152]. Besides, microstructural heterogeneities associated with AM-based parts have been reported to promote shear-induced failure during compressive deformation of AM-based components [152]. Additionally, the difference between real and virtual design (CAD-based) of AM components may lead to detrimental consequences (during component fabrication) [147, 148]. For instance, during DED (discussed in section 2.3), the major limitation is that may not be captured the internal features of a component accurately during CAD-based virtual design [149]. This may lead to the rough surface finish of the final component [150]. Besides, the other drawback of AM-based methods is the trapping of the support material between internal surfaces during layered deposition (in AM-based methods) [147]. This has been reported to degrade the load-bearing capacity of AM-based components [151, 152]. However, this problem is more significant in the case of metallic components manufactured using AM-based techniques.

Although a number of ways for minimisation of cracking and enhancement of density (of the final part) along with mechanical properties of AM based ceramics have been devised [22], however, these post-processing techniques have failed to render these materials as suitable candidates for high performance applications in the aforementioned sectors, unlike that of conventionally fabricated ceramic parts. This necessitates an understanding of microstructures in AM-based ceramic and cermet parts through a systematic structure-property correlation using extensive structural cum chemical characterisation techniques.

Liu *et al* [153] have studied the influence of scanning speed (of laser) on the solidification of $Al_2O_3/GdAlO_3/ZrO_2$ ternary eutectic ceramics during SLM. It has been reported that a scanning speed of $\sim$ 12 mm/min reduced the volume fraction of solidification defects such as cracks and pores (figure 16) [153]. Besides, the relative density of the

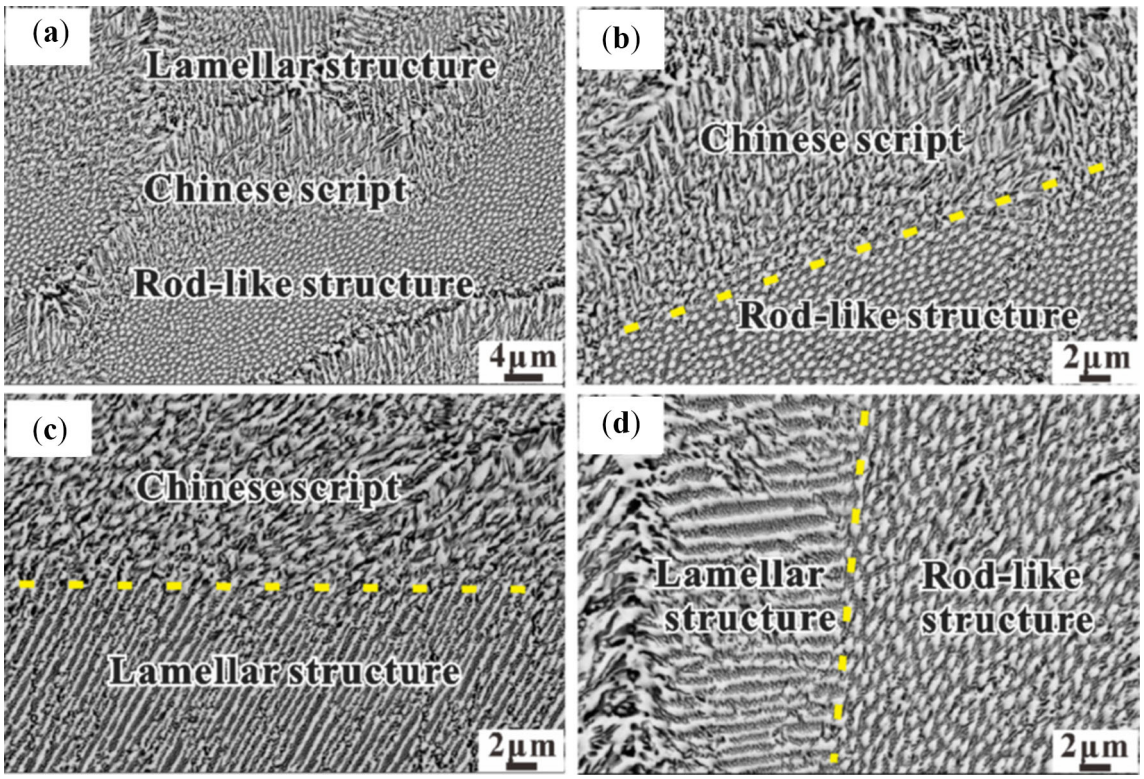

Figure 12. **(a)** Morphological transitions in the microstructure of SLM-based Al_2O_3/GAP/ZrO_2 eutectic ceramic, **(b)** transition from "Chinese-script" to rod-like eutectic morphology, **(c)** transition from "Chinese script" to lamellar eutectic morphology and **(d)** transition from lamellar eutectic structure to rod-like eutectic morphology. GAP abbreviates for Al_2O_3/$GdAlO_3$ eutectic phase [147] .

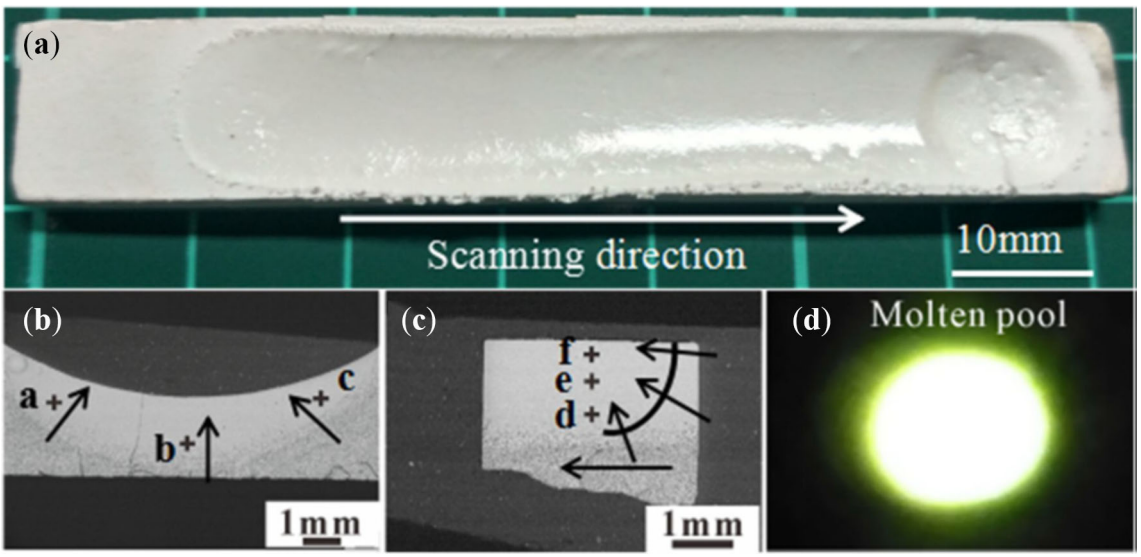

Figure 13. **(a)** As-solidified Al_2O_3/GAP/ZrO_2 eutectic sample, **(b)** Transverse section, **(c)** Longitudinal section, and **(d)** Molten pool [147].

aforementioned ternary eutectic decrease from ∼98.7 to ∼95.4%, with an increase in scanning speed to 48 mm/min [153].

Eutectic spacing (in the top zone of the molten pool) has also been reported to decrease initially with increasing laser scanning speed from 6 mm/min to 12 mm/min and then

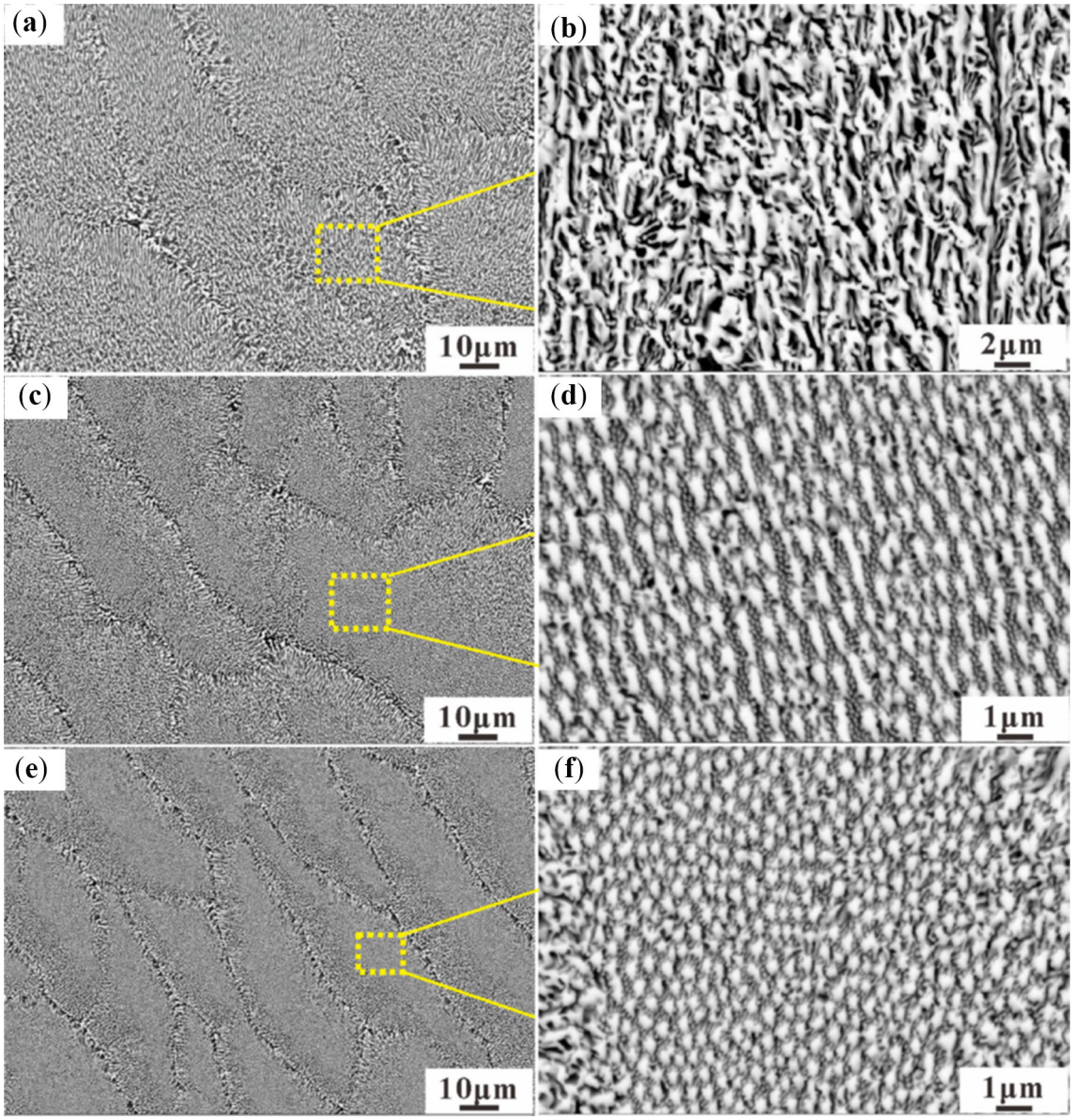

Figure 14. SEM images at different regions of the melt pool: **(a and b)** bottom-zone, **(c and d)** middle zone, and **(e and f)** top-zone [147].

undergo a subsequent increase with increasing scanning speed till 48 mm/min [153] (figure 17). This has been attributed to the dominance of laser scanning speed as a significant influencing factor during solidification for SLM. Liu *et al* [154] have reported the influence of high-temperature (∼1500-2500°C) preheating on the SLM of YSZ. It has been reported that with increasing preheating temperature from 1500 to 2500°C, there is a modification of crack morphology of YSZ [154]. Vertical cracks, in particular, have been reported to undergo shortening, which prevents their coalescence leading to restricted propagation (between the adjacent layers) along the same scanning direction (of the laser during SLM) (figure18) [154].

Recently, Liu *et al* [155] have reported the synthesis of $Al_2O_3/GdAlO_3/ZrO_2$ ternary eutectic ceramics using laser directed energy deposition (LDED) technique. The microstructure was reported to comprise periodic banded structures (figure 19), and this was attributed to abnormal coarsening occurring close to the melt pool. Figures 19 (a and b) show the and microstructure at low and high magnifications, respectively. Based on partial remelting using a CO_2 laser, it has been reported that microstructural coarsening zone (MCZ) exists only in regions where a fine initial (the term "initial" refers to the state before laser remelting) eutectic structure is present (figures 19(c and d)) [155]. However, there is no MCZ in regions where a coarse initial

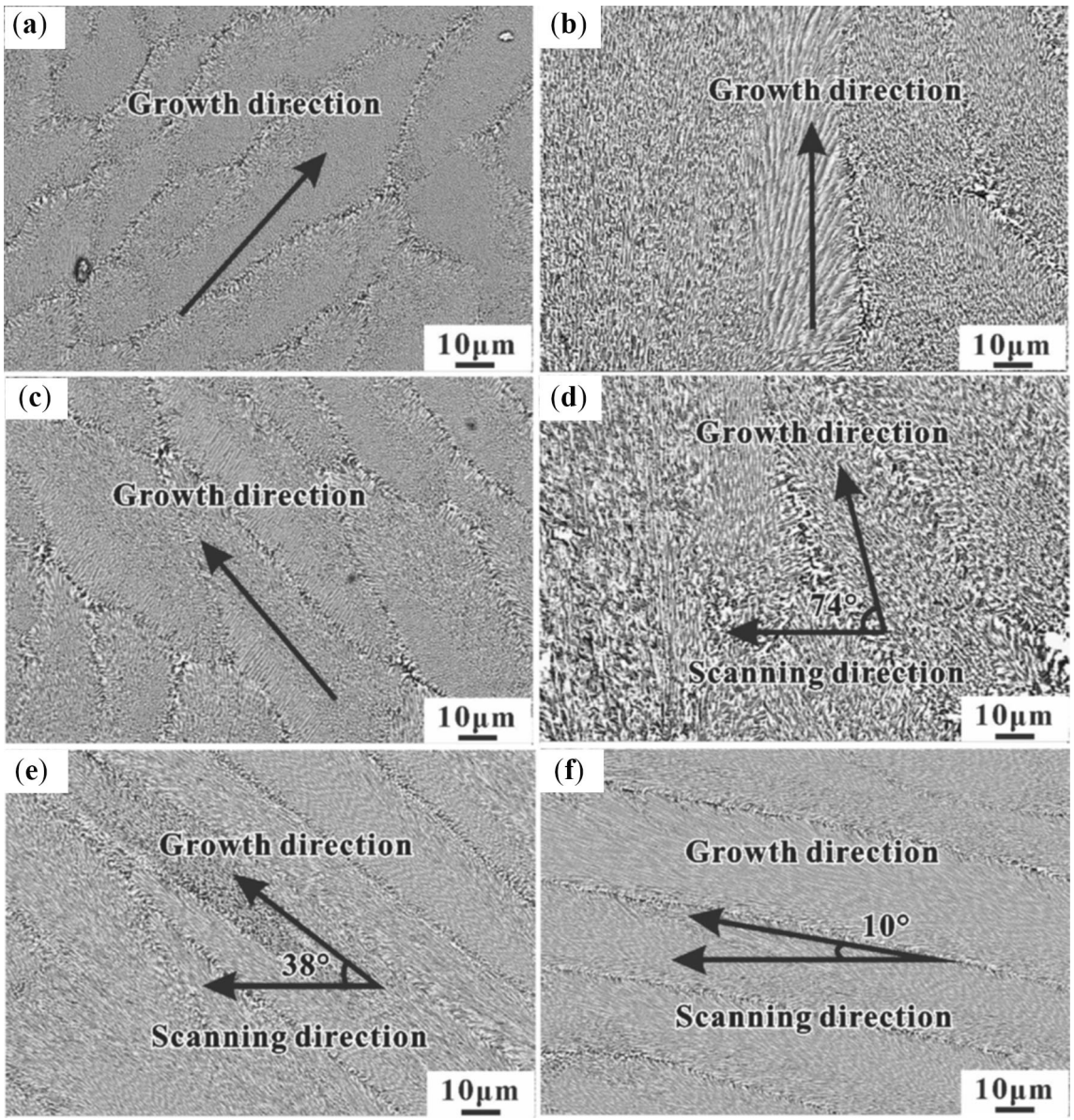

Figure 15. SEM images showing microstructure growth directions at different regions of the melt pool: **(a)** left boundary, **(b)** bottom boundary, **(c)** right boundary, **(d)** bottom zone, **(e)** middle zone, **(f)** top zone [147].

eutectic structure is present (figures 19(e and f)) [155]. The formation of MCZ has been attributed to the microstructural coarsening behavior observed during fabrication. An initially fine eutectic structure tends to undergo coarsening to minimizing its interfacial energy [155]. In this context, the finer the initial eutectic structure, the higher is the driving force for coarsening. Based on the aforementioned study [155], it has been proposed that during solidification of the melt pool (during LDED), there is nucleation and growth of crystals leading to a branched microstructure in the upper boundary of the MCZ. Fan *et al* [156] have reported the presence of a periodically banded microstructure of nanostructured Al_2O_3-YAG-ZrO_2 (AYZ) ternary eutectic ceramic fabricated using laser engineered net shaping (LENS). It has been reported that in each solidified layer, there is a microstructural transition from planar to cellular morphology along the building direction (BD) [156]. The characteristic dimensions achieved during microstructural evolution have been reported to possess an excellent correlation with the Jackson-Hunt relationship [156]. Figure 20 shows Transmission Kikuchi Diffraction (TKD)-based inverse pole Figure (IPF) maps and the corresponding pole Figures of Al_2O_3, YAG, and ZrO_2 phases. An electron transparent lamella extracted from a cellular region in the central portion of the AYZ eutectic using Focussed Ion Beam (FIB)-based lift-out technique. Figure 21 shows high-resolution transmission electron microscopy (HRTEM) image of a triple junction (TJ) between

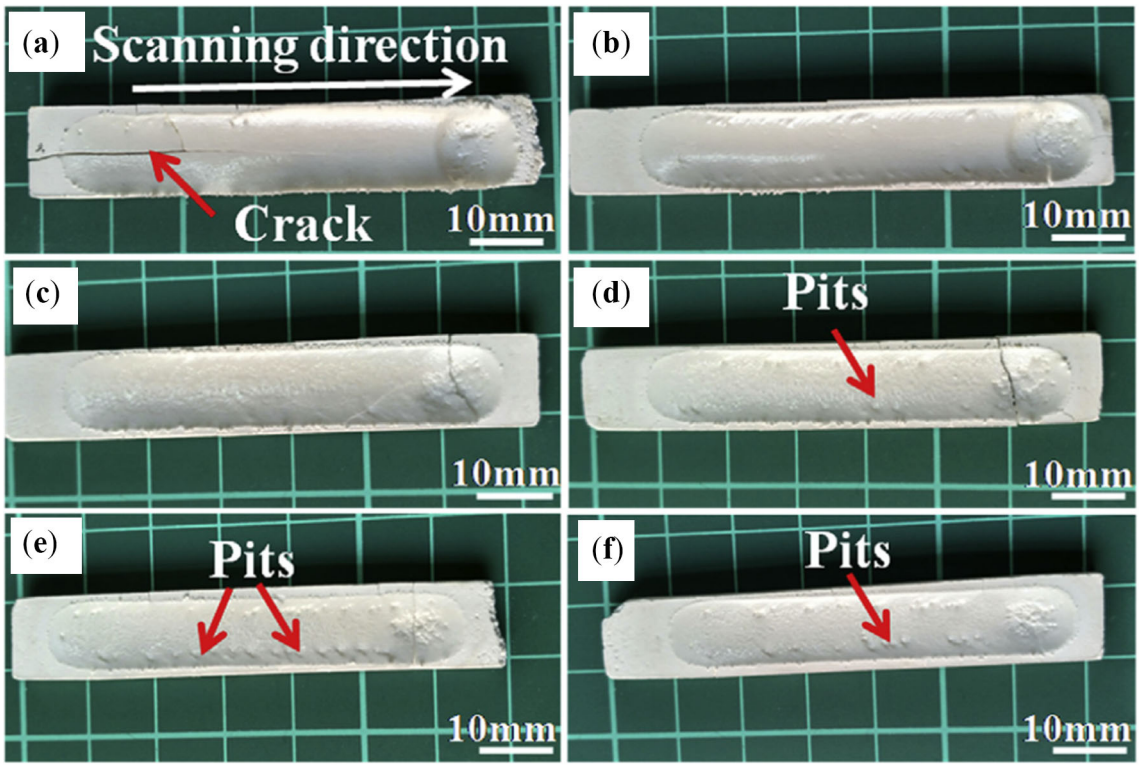

Figure 16. SLM-based Al_2O_3/GAP/ZrO_2 ternary eutectic samples under different laser scanning speeds: **(a)** 6 mm/min, **(b)** 12 mm/min, **(c)** 18 mm/min, **(d)** 24 mm/min, **(e)** 30 mm/min, and **(f)** 48 mm/min [153].

Al_2O_3, YAG, and ZrO_2 phases along the transverse section and the corresponding Fast Fourier Transform (FFT)-based diffraction pattern in LENSed AYZ eutectic ceramic. Both figures 20 and 21 suggest that an orientation relationship (OR) of $<0001>_{Al2O3} \parallel <001>_{YAG} \parallel <001>_{ZrO2}$ at the interior of LENSed eutectic region along BD, but there is a deviation (deviation of $(200)_{YAG} \sim 3°$ with respect to $(11\text{-}20)_{Al2O3}$ and $(002)_{ZrO2}$) in the aforementioned OR due to a transition from planar to cellular morphology of the LENSed AYZ eutectic (from center to edge of the specimen) [156]. In addition, ffigure 20 also shows that there is a strong coherence at TJ between Al_2O_3, YAG, and ZrO_2 phases. Both Al_2O_3/ZrO_2 and YAG/ZrO_2 interfaces have been reported to possess a lower extent of lattice disregistry as compared to that of the Al_2O_3/YAG interface [157–159], suggesting that the dispersion of the ZrO_2 phase must contribute to the atomic matching in the LENSed AYZ specimen. Figure 22 shows the TKD-based analysis of a longitudinal section of LENSed AYZ specimen extracted using the FIB-based lift-out technique in SEM. Figure 22 indicates that the primary growth direction of the cellular microstructure in LENSed AYZ eutectic ceramic is $<0001>_{Al2O3} \parallel <001>_{YAG} \parallel <001>_{ZrO2}$. The LENSed eutectic specimen has been reported to exhibit nearly isotropic properties with Vickers microhardness and fracture toughness values of $\sim 18.9 \pm 0.96$ GPa and 3.84 ± 0.44 MPa $m^{1/2}$, respectively along the longitudinal section and $\sim 18.73 \pm 0.94$ GPa and 3.53 ± 0.32 MPa $m^{1/2}$, respectively along the transverse section. These values were almost comparable with those of the AYZ eutectic ceramics fabricated using conventional techniques [156]. Table 6 shows typical ceramics (both structural and functional) and cermets manufactured using different AM-based techniques.

As discussed earlier, the onset of "Correlative Microscopy" involving both structural and chemical characterisation from the same region in the microstructure [25–30], in recent times, has provided a major breakthrough in understanding a number of different properties in different metallic materials [25–30]. However, at present, there is hardly any report on understanding the mechanical properties of AM-based ceramic and cermet parts using the aforementioned approach. In this regard, it becomes highly essential to mention about the role of different 2D interfaces in influencing the mechanical properties of these materials. The simplest of the 2D interfaces in crystalline ceramics (and even cermets) are grain boundaries (GBs) and interphase boundaries (IBs) (for multiphase materials). In the context of metallic materials, during plastic deformation, stress concentration at GBs and IBs (both mechanically "weaker" as compared to the lattice) leads to intergranular fracture [157–167]. This is the most common

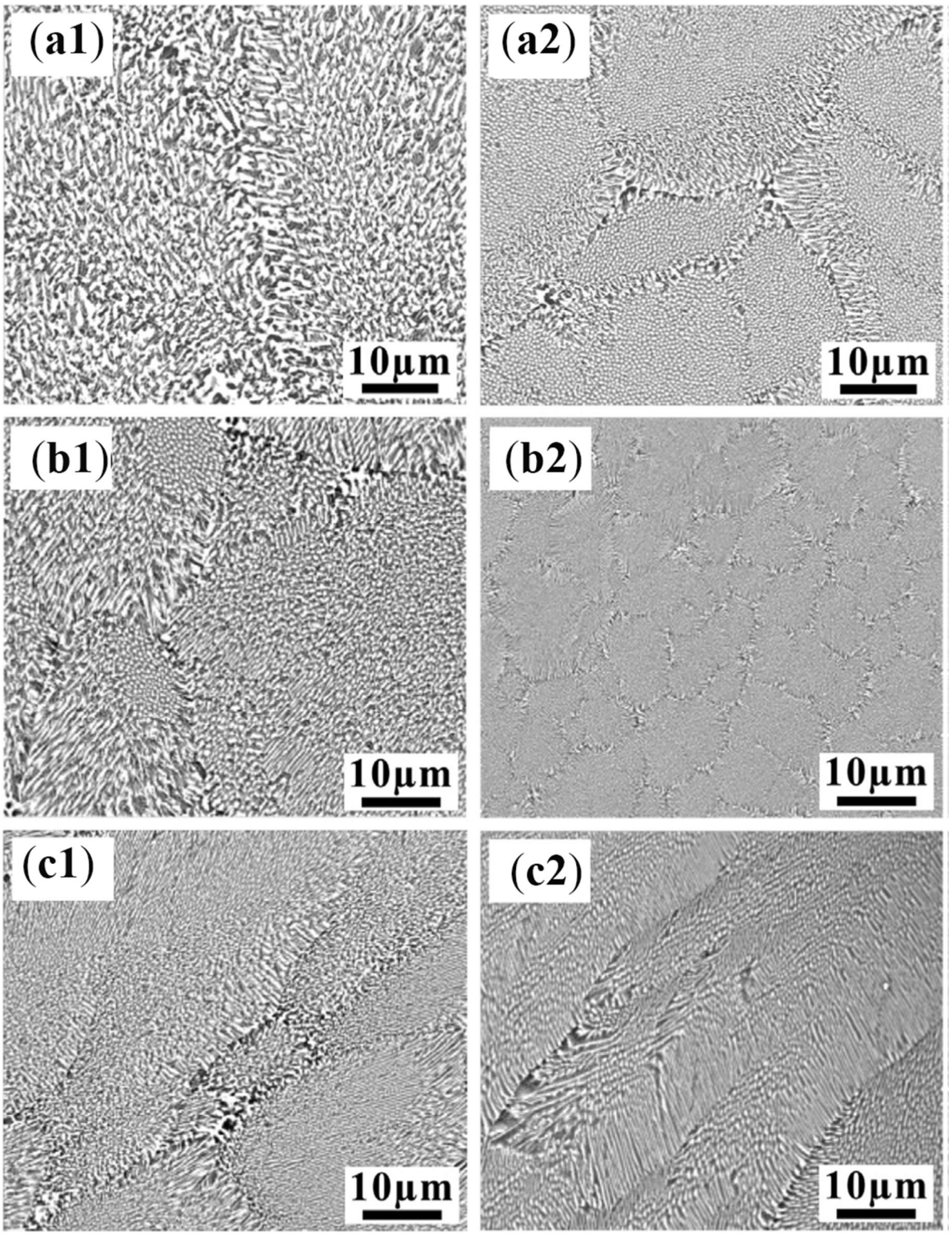

Figure 17. SEM-based images at different zones of the melt pool with various laser scanning speeds (during SLM): (**a1) - (a2)** 6 mm/min, **(b1) - (b2)** 12 mm/min, and **(c1) - (c2)** 48 mm/min, where 1 and 2 represent the bottom and the top zones (of the melt pool), respectively [153].

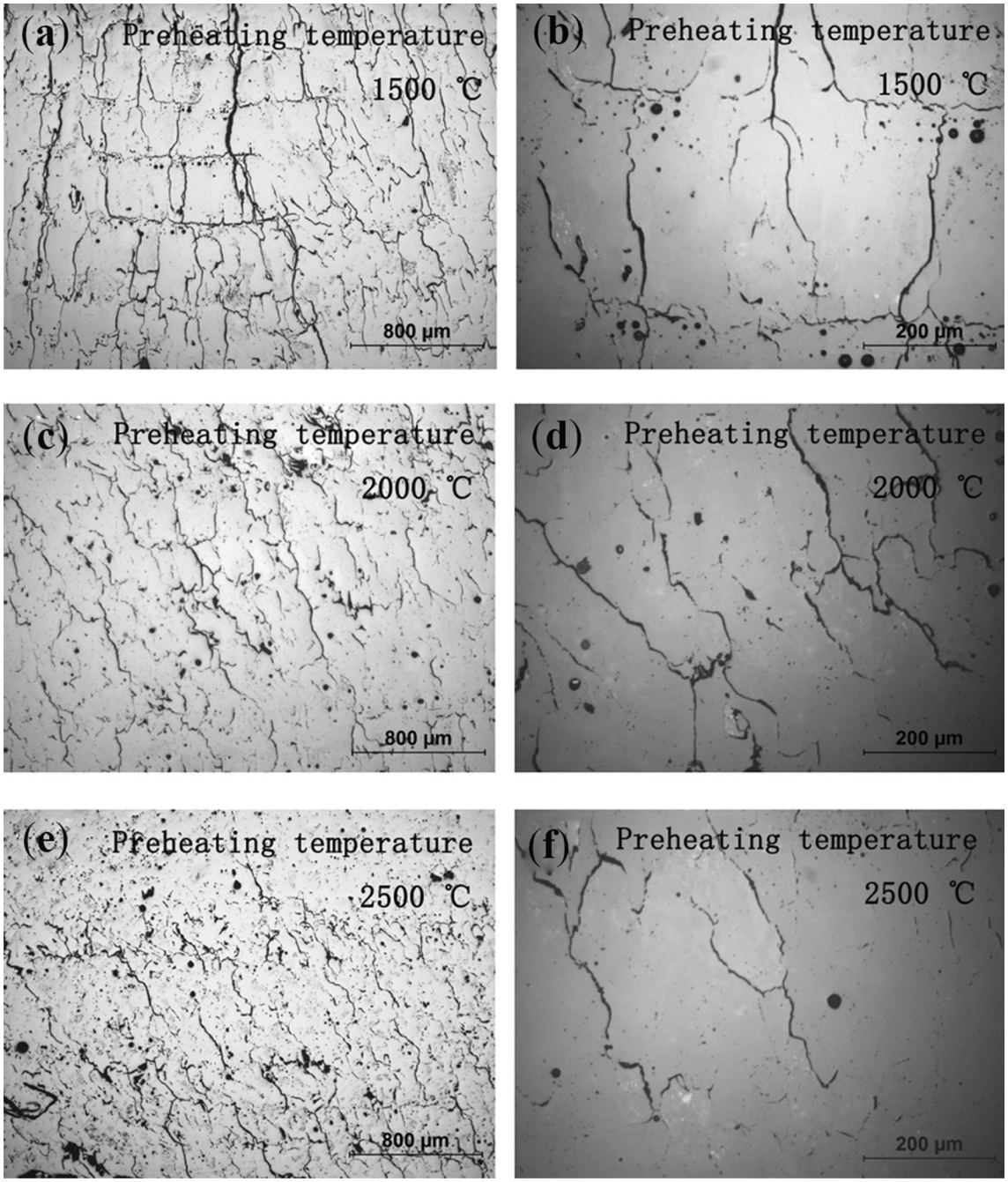

Figure 18. Influence of different preheating temperatures on the microstructure of SLM-processed YSZ: **(a and b)** 1500°C, **(c and d)** 2000°C, and **(e and f)** 2500°C [154].

mode of failure in metallic materials during service [151, 164]. Moreover, in the context of metallic materials, it has been reported that by controlling the fraction of different GBs in the microstructure (also reported as "GB engineering" (GBE) in many literatures), it is possible to engineer mechanical properties [164–188]. However, for AM-based crystalline ceramics and cermets with low-symmetry crystal structures, the structure of GBs and IBs tends to be much more complex as compared to those in metallic materials which mainly comprise of high-symmetry crystal structures [156]. This has been the main reason as to why there is hardly any report on GBE of AM-based ceramics and cermets.

Thus, in addition to optimisation of different processing parameters, "Correlative microscopy" approach may be utilised for a systematic structure-property correlation combined with tailoring of microstructures in these materials based on GBE, in order to overcome the problem of

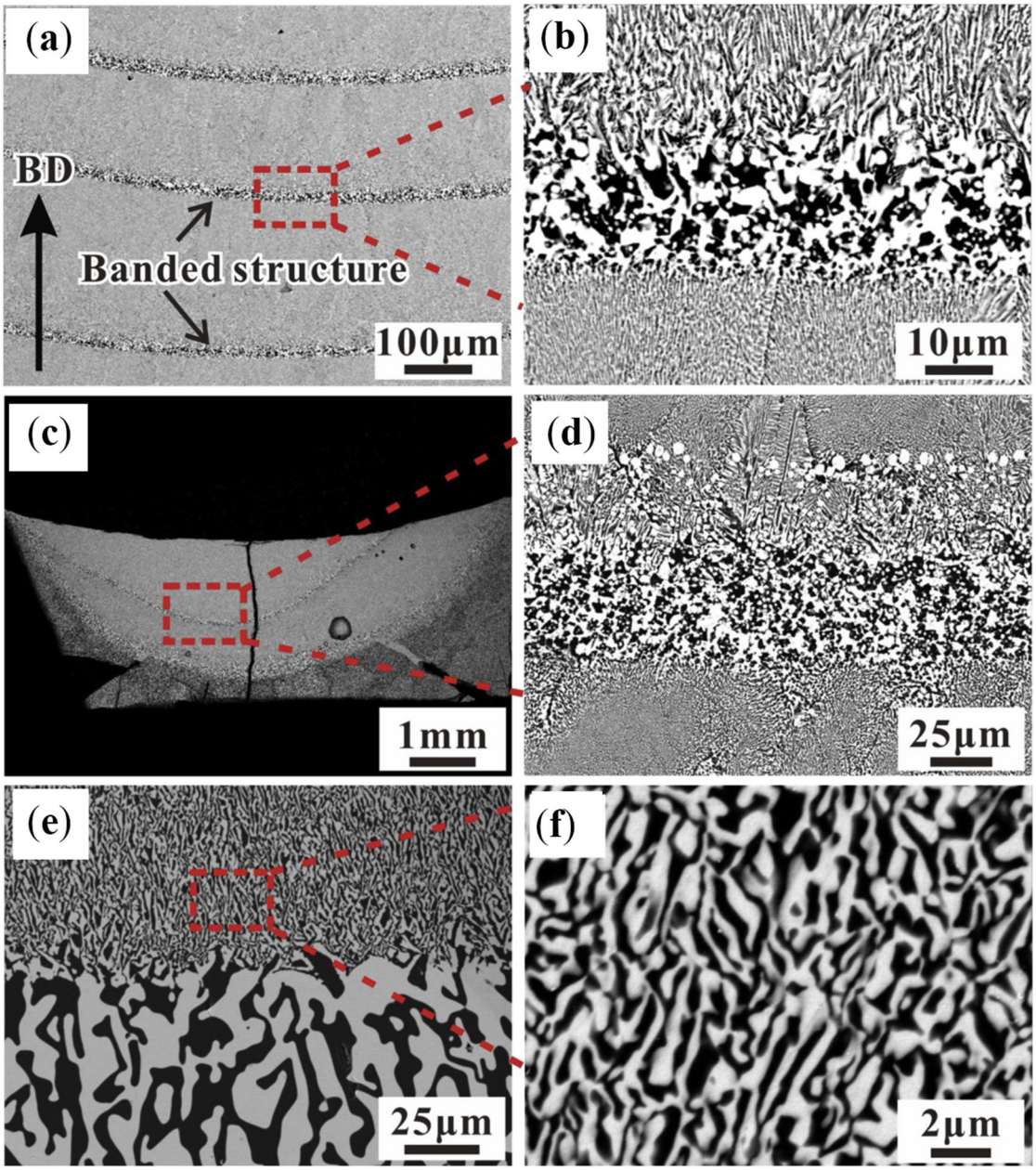

Figure 19. **(a and b)** The as-synthesized LDED-processed $Al_2O_3/GdAlO_3/ZrO_2$ eutectic sample, **(c and d)** the partial-laser-remelted eutectic sample with a fine initial eutectic structure, and **(e and f)** partial-laser-remelted eutectic sample with a coarse initial eutectic structure [155]. The term "initial" refers to the state before laser remelting.

poor mechanical properties in AM-based ceramics and cermets. Moreover, this avenue is presently unexplored and hence, offers a great potential for future investigations.

5.3 *From the authors' viewpoint*

As rightly highlighted by Zocca *et al* [144], AM-based techniques enable the fabrication of porous ceramic parts with complex geometries with a high level of accuracy, which is not achievable by any present traditional fabrication technique. However, the AM-based techniques suitable for fabricating fine porous ceramic components face a major challenge in bulk scale. Similarly, the AM-based techniques face difficulties for fabricating dense and bulk components [156–165, 172, 173]. Moreover, there are very few commercially available AM-based techniques for the

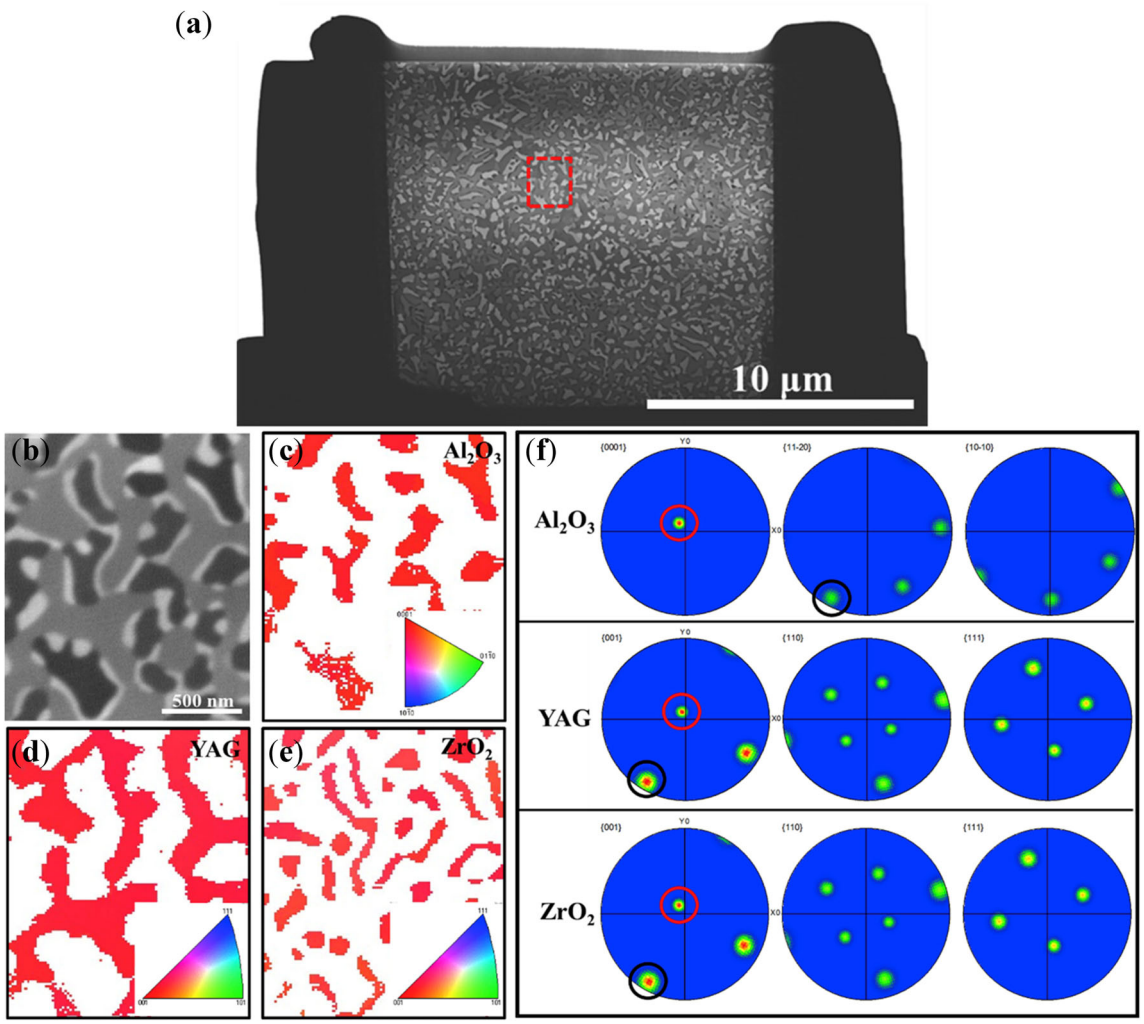

Figure 20. **(a)** Field-Emission (FE)-SEM image of the electron transparent lamella of a transverse section of the LENSed AYZ sample prepared using FIB-based lift-out technique in SEM, **(b)** TKD analysis of the region inside cellular eutectic (indicated using a red-dotted square in part **(a)**); **(c, d, and e)** TKD-based IPF maps of Al_2O_3, YAG and ZrO_2 phases respectively, and **(f)** pole Figures of Al_2O_3, YAG and ZrO_2 phases corresponding to (c), (d) and (e), respectively [156].

fabrication of fully dense monolithic ceramic parts [144]. This still remains a major scientific challenge and needs to be addressed in order to promote AM of ceramics for large-scale industrial applications. As discussed earlier (in sections 5.1 and 5.2), the other challenges associated with AM of ceramics include high processing costs (even for small-scale production), complex machining, and low flexibility. Besides, many of the challenges involved with AM of ceramics are also associated with the traditional ceramic fabrication techniques.

The aforementioned practice in the field of AM-based ceramic research may solve most of the processing-based challenges for structural and functional ceramics and even cermets. However, the other major obstacle is the limited interaction between the industry and academia in the above context. This mainly leads to challenges in terms of material properties during upscaling of AM-based ceramic parts from laboratory to industrial scale and even during the downscaling of dense and bulk AM-based ceramic parts to laboratory-scale prototypes. Therefore, both industry and academia must make a combined effort (of multidisciplinary nature) towards a systematic understanding of the structure-property correlation to solve the challenge mentioned earlier. This is one of the areas where the correlative methodology of material characterization (ranging from bulk to atomic scale) may be employed as a potential tool to obtain both structural and chemical information.

The same region in a given microstructure (as extensively discussed in section 5.2), thereby enabling one to explore different microstructural defects (evolved during AM) in extensive details and new perspectives. However, the primary challenges in the avenue of correlative

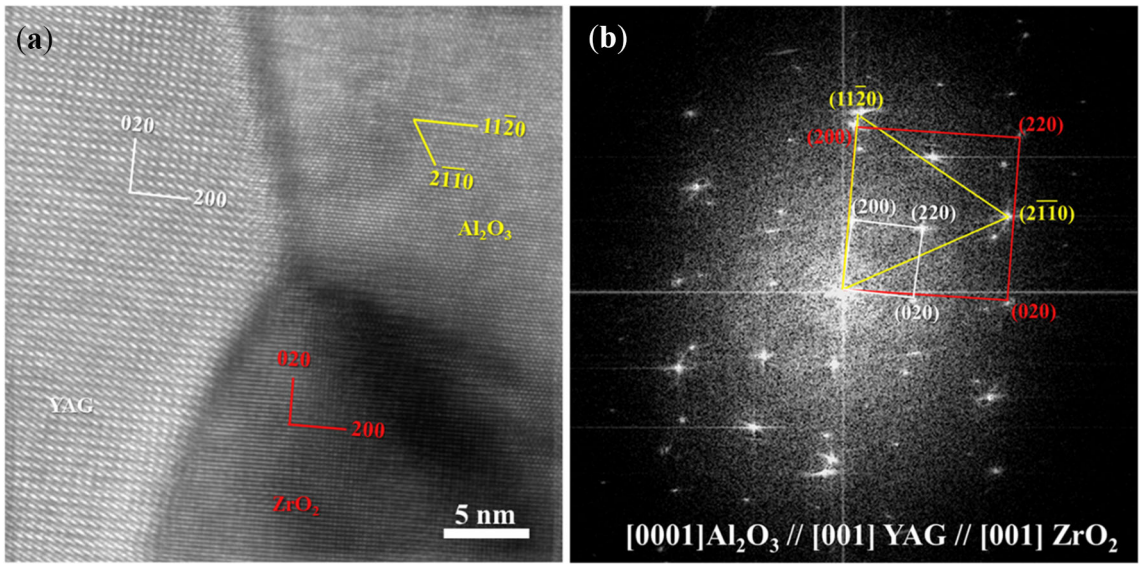

Figure 21. **(a)** HRTEM image of the transverse section in LENSed AYZ eutectic showing a triple junction between Al_2O_3, YAG, and ZrO_2 phases, and **(b)** Corresponding FFT diffraction pattern with zone axis: [0001] $_{Al2O3}$ ‖ [001] $_{YAG}$ ‖ [001]$_{ZrO2}$ [156].

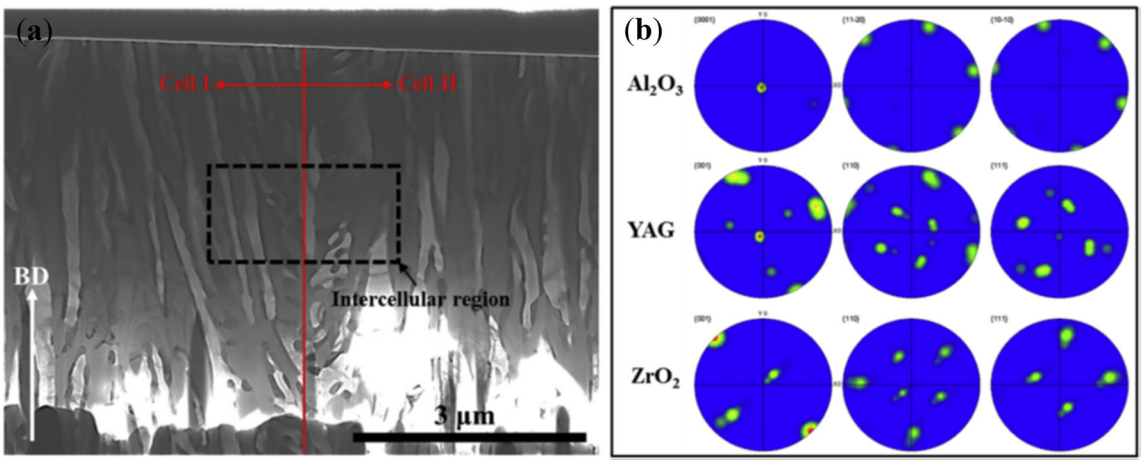

Figure 22. TKD analysis of the electron transparent lamella extracted from the longitudinal section of the LENSed AYZ specimen using FIB-based lift-out technique in SEM: **(a)** FE-SEM image, and **(b)** TKD-based pole Figures of Al_2O_3, YAG, and ZrO_2 phases based on multiple scanning in the intercellular region highlighted using black dotted rectangle in part **(a)** [156]**.**

characterization are the requirement of high-end characterization techniques and the expertise to capture the required micrstructural features. Besides, the other challenge associated with the aforementioned characterization methodology is the lack of repeatability associated with the visualization of nanoscale features throughout the entire microstructure. This is especially significant for AM-based components (metallic materials, ceramics, and polymers) in which the non-equilibrium processing conditions (during AM) lead to large-scale microstructural heterogeneities.

Unlike AM of ceramics, AM of metals (a more mature technology at present) suffers from the limitation in terms of availability of raw materials for feedstock production [144, 155]. Ceramic powders for almost all-ceramic systems are commercially available. The molds used for forming ceramic parts are highly expensive. They require a large number (of the order of a few thousand) of components to be fabricated before becoming cost-effective [144]. However, the market demands only a single piece with the size (of a lot) typically varying between 10 and 20 parts [155], which necessitates CAD/CAM processing followed by the machining of green components (ceramic components) [152]. Despite the emergence of a large number of AM-based techniques for the fabrication of ceramics and

Table 6. Common AM-based techniques for the fabrication of ceramics and cermets (abbreviations: PE: Polyethylene, PZT: Lead zirconium titanate, LSMO: Lanthanum strontium manganite, YBCO: Yttrium barium copper oxide, RO: Alkaline oxide (R: Alkali), ITO: Indium tin oxide, PMN: Lead magnesium niobate, YSZ: Yttria-stabilised Zirconia)

Material	3DP	SLS®	SLA	FEF	LOM	SLM	LENS	DLF
Structural ceramics	ZrO_2 [22, 35–39] Al_2O_3 [36, 37] Ti_3SiC_2 [37–40] Si_3N_4 [41, 42] TiC-TiO_2 [43–45] SiC [46]	ZrO_2 [40–44] Al_2O_3 [45] Al_2O_3-SiO_2 [17] TiC-Al_2O_3 [60–62] ZrB_2 [90, 91, 97–99] SiC [92]	Al_2O_3 [44] Al_2O_3-ZrO_2 [53–58] Al_2O_3-SiO_2 [68] SiO_2 [69–73] TiO_2 [80] SiC [81] Mullite [87] $ZrSiO_4$ [87]	Al_2O_3 [41] ZrB_2 [48] HfB_2[50] (fabricated using conventional Robocasting technique) Mullite [75] SiC [78] Si_3N_4 [81–87] ZrO_2 [37] WC-ZrO_2 [54] ZrC [60] Al_2O_3-ZrO_2 [68]	Al_2O_3 [36] ZrO_2 [56] SiC/C [78] PE-glassy fiber [77, 79] Si_3N_4 [80] SiO_2 [81–83, 105–111]	Al_2O_3-$GdAlO_3$-ZrO_2 [147] YSZ [154]	ZrB_2 [130] Al_2O_3-YAG-ZrO_2 [156]	
Functional ceramics	$BaTiO_3$ [85] PZT [50–52] TiO_2 [54] YBCO [55] LSMO [54–57]	$BaTiO_3$ [84, 85] PZT [95]	SiCN [89–94] PZT [95] Fe_2O_3 [96–99] $Fe(C_2O_4)$ [99] $Bi(V_xNb_{1-x})O_4$ [100–103, 112, 118] SiCN [104, 119–126]	$BaTiO_3$ [85] PZT [93] PMN [83] $LiFePO_4$ [86] $Li_4Ti_5O_{12}$ [88] $BaZrO_3$ [87], $SrTiO_3$ [85] ZnO [82] ITO [82] $BaMn_2Al_{10}O_{19-x}$ [83] TiO_2 [44] $Zr_{0.8}Sn_{0.2}TiO_4$ [81] $La(Mg_{0.5}, Ti_{0.5})O_4$ [79]	SiO_2-Al_2O_3-RO-glass [118] LZSA [118] PZT [117]			
Cermets	WC-Co [139] (Ti(C,N), WC,(Ta,Nb)C, Cr_3C_2)-Co, Ni [137, 138]	WC-Co/Cu [121–126]				WC-Co [118–120]	WC-Co [125]	TiC-Ni [128]

cermets, the main problem (at present) lies in the coupling of a specific AM-based technique with a proper feedstock formulation for the purpose of enabling the fabrication of dense ceramic components with optimal properties (mechanical strength, surface finish, etc.).

Powder-based AM techniques have a much higher potential for extensive applications in the immediate future when compared to the other AM-based techniques using solid-sheet, paste, or liquid as starting materials [155, 156] (shown in table 4). They are owing to the low processing cost coupled with easy scalability (to bulk and dense components) and parallel processing of multiple components. However, the major challenge with powder-based AM techniques that still remains to be solved is the low packing density and stability of dry powders for dry powders (used as feedstock), which necessitates support structures. Zocca *et al* [144] have proposed replacing dry powders with ceramic slurries (with ceramic powder sizes ranging from <100 nm to >100 nm) as a solution to the problem as mentioned above. Besides, the above solution (proposed in Ref. [144]) is already in use in the SLS technique. Hence, in the near future, the SLS technique is the only AM technique that may be expected to dominate global ceramic markets. On the other hand, based on the report of Qian and Shen [174], Laser sintering as an AM-based fabrication technique is suitable for rapid prototyping and the synthesis of a wide range of materials (including metallic materials, plastics, and ceramics). However, in plastics and metallic materials, Laser sintering is a more mature technology than that for ceramics. At present, a number of Laser sintering techniques are commercially for the construction of complex 3D components. Laser sintering techniques offer a number of advantages, including fabrication of ceramics with non-equilibrium phases with hierarchically structured heterogeneities (not achievable by any conventional sintering technique) [174]. Besides, these techniques enable the sintering of very high-melting ceramics (including transition metal boride-based UHTCs). At present, minimization of residual thermal stresses during Laser sintering in ceramics is a major scientific challenge. Besides, attaining extremely low dimensional tolerances for fabricating micrometer-scale components is another significant challenge in the context of Laser sintering of ceramics. These two aforementioned challenges need to be extensively addressed to render Laser sintering techniques suitable for large-scale industrial production of complex ceramic components. At present, large-scale commercial use of AM-based techniques for ceramic fabrication remains a major challenge. The solutions (proposed recently) towards the fabrication of dense monolithic ceramic parts [22, 35–40, 172–175, 189–197] are most likely to deviate from the powder processing techniques followed by the traditional ceramic fabrication techniques.

6. Conclusions

There remains absolutely no doubt that AM based techniques for fabrication of ceramics and cermets are likely to benefit from close collaborative research between the academia and industry. However, optimisation in processing parameters coupled with a proper understanding of structure-property correlation in AM based ceramic parts, is crucial for a complete utilisation of the enormous potential (both in terms of academic and industrial research) offered by these materials and aiming towards their mass production.

Abbreviations

3DGP	3D Gel Printing
3DFD	3D fibre deposition
AFM	Atomic Force Microscopy
AJP	Aerosol jet printing
AM	Additive manufacturing
AYZ	Alumina-Yttria-Zirconia
BJ3DP	Binder jet 3D printing
BSE	Back scattered electron
CAD	Computer-aided design
CAM	Computer-aided manufacturing
CEM	Composite-extrusion modeling
CLG	Ceramic laser gelling
CLS	Ceramic laser sintering
CIB	Chemically induced bonding
CODE	Ceramic-on demand extrusion
DED	Directed energy deposition
DLD	Direct laser deposition
DLF	Direct laser fabrication
DMLS	Direct metal laser sintering
EBM	Electron beam melting
EBSD	Electron Backscatter Diffraction
EBW	Electron beam welding
EDS	Energy Dispersive Spectroscopy
EFF	Extrusion free forming
EPD	Electrophoretic deposition
FDC	Fused deposition of ceramics
FDM	Fused deposition modeling
FEF	Freeze-form extrusion fabrication
FFF	Fused Filament Fabrication
FFT	Fast Fourier Transformation
FIB	Focussed Ion Beam
GAP	Gaolinia-alumina eutectic
GB	Grain boundary
GBE	Grain boundary engineering
HIP	Hot isostatic pressing
HRTEM	High-resolurion Transmission Electron Microsopy

IB	Interphase boundary
IJP	Inkjet printing
IPF	Inverse pole figure
ITO	Indium tin oxide
LAMP	Large Area Maskless Photopolymerization
LCM	Lithography based Ceramic Manufacturing
LDED	Laser directed energy deposition
LEM	Laminated Engineering Materials
LENS	Laser engineered net shaping
LOM	Laminated object manufacturing
LPS	Liquid phase sintering
LSMO	Lanthanum strontium manganite
MCZ	Microstructural coarsening zone
MIM	Metal injection molding
MJS	Multiphase jet solidification
MMC	Metal matrix composite
OR	Orientation relationship
P-3DP	Powder-based three-dimensional printing
PE	Polyethylene
PIM	Powder injection molding
PMN	Lead magnesium niobate
PVA	Polyvinyl alcohol
PZT	Lead zirconium titanate
RO	Alkaline oxide (R: Alkali)
S-3DP	Slurry based three-dimensional printing
SEM	Scanning Electron Microscopy
SLA	Stereolithography
SLM	Selective laser melting
SLRS	Selective laser reactive sintering
SLS	Selective laser sintering
SSS	Solid state sintering
TJ	Triple junction
TKD	Transmission Kikuchi Diffraction
UHTC	Ultra high temperature ceramic
UHTCMC	Ultra high temperature ceramic matrix composite
XRD	X-ray Diffraction
YAG	Yttrium Aluminium Garnet
YBCO	Yttrium barium copper oxide
YSZ	Yttria stabilised Zirconia
ZTA	Zirconia (ZrO_2) toughened alumina (Al_2O_3

Acknowledgement

MS would like to thank his undergraduate research supervisor Dr. MM, for his guidance and continuous support during the drafting of the manuscript.

References

[1] Conrad H J, Seong W J and Pesun I J 2007 Current ceramic materials and systems with clinical recommendations: a systematic review. *J. Prosthet. Dent.* 98: 389–404

[2] Blatz M B, Sadan A and Kern M 2003 Resin-ceramic bonding: a review of the literature. *J. Prosthet. Dent.* 89: 268–274

[3] Kingery W D 1955 Factors affecting thermal stress resistance of ceramic materials. *J. Am. Ceram. Soc.* 38: 3–15

[4] Cao X Q, Vassen R and Stoever D 2004 Ceramic materials for thermal barrier coatings. *J. Eur. Ceram. Soc.* 24: 1–10

[5] De Aza A H, Chevalier J, Fantozzi G, Schehl M and Torrecillas R 2002 Crack growth resistance of alumina, zirconia and zirconia toughened alumina ceramics for joint prostheses. *Biomaterials.* 23: 937–945

[6] Akhtar F, Rehman Y and Bergström L 2010 A study of the sintering of diatomaceous earth to produce porous ceramic monoliths with bimodal porosity and high strength. *Powder Technol.* 201: 253–257

[7] Wu J M, Lu W Z, Lei W, He J P and Wang J 2011 Effects of aqueous gel-casting and dry pressing on the sinterability and microwave dielectric properties of $ZnAl_2O_4$-based ceramics. *Ceramics Int.* 37: 481–486

[8] Wu J M, Lu W Z, Wang X H, Fu P, Ni M, Yang J L, Wang C and Zeng Q C 2013 $Ba_{0.6}Sr_{0.4}TiO_3$-MgO ceramics from ceramic powders prepared by improved aqueous gel casting-assisted solid-state method. *J. Eur. Ceram. Soc.* 33: 2519–2527

[9] Chen A N, Wu J M, Liu M Y, Cheng L J, Chen J Y, Xiao H, Zhang X Y, Li C H and Shi Y S 2017 Rapid in-situ solidification of SiO_2 suspension by direct coagulation casting via controlled release of high valence counter ions from calcium iodate and pH shift. *Ceram. Int.* 43: 1930–1936

[10] Sebastian M T, Ubic R and Jantunen H 2015 Low-loss dielectric ceramic materials and their properties. *Int. Mater. Rev.* 60: 392–412

[11] Zhang X and Zhao L D 2015 Thermoelectric materials: energy conversion between heat and electricity. *J. Materiomic.* 1: 92–105

[12] Simonenko E P, Sevast'yanov D V, Simonenko N P, Sevast'yanov V G and Kuznetsov N T 2013 Promising ultra-high-temperature ceramic materials for aerospace applications. *Russ. J. Inorg. Chem.* 58: 1669–1693

[13] Baklouti S, Bouaziz J, Chartier T and Baumard J F 2001 Binder burnout and evolution of the mechanical strength of dry- pressed ceramics containing poly(vinyl alcohol). *J. Eur. Ceram. Soc.* 21: 1087–1092

[14] Trunec M, Klimke J and Shen Z J 2016 Transparent alumina ceramics densified by a combinational approach of spark plasma sintering and hot isostatic pressing. *J. Eur. Ceram. Soc.* 36: 4333–4337

[15] Jabbari M, Bulatova R and Tok A I Y, Bahl C R H, Mitsoulis E, Hattel J H 2016 Ceramic tape casting: a review of current methods and trends with emphasis on rheological behaviour and flow analysis. *Mater. Sci. Eng. B.* 212: 39–61

[16] Beaman J J and Deckard C R 1990 Selective laser sintering with assisted powder handling. *United States patent* 4(938): 816

[17] Wu Y, Du J, Choy K L and Hench L L 2007 Laser densification of alumina powder beds generated using aerosol assisted spray deposition. *J. Eur. Ceram. Soc.* 27: 4727–4735

[18] Wu Y, Du J, Choy K L and Hench L L 2007 Fabrication of titanium dioxide ceramics by laser sintering green layers prepared via aerosol assisted spray deposition. *Mater. Sci. Eng. A.* 454–455: 148–155

[19] Zhu W, Yan C, Shi Y, Wen S, Liu J and Shi Y 2015 Investigation into mechanical and microstructural properties of polypropylene manufactured by selective laser sintering in comparison with injection molding counterparts. *Mater. Des.* 82: 37–45

[20] Ma A, Roters F and Raabe D 2006 Studying the effect of grain boundaries in dislocation density based crystal plasticity finite element simulations. *Int. J. Solids Struct.* 43: 7287–7303

[21] ISO/ASTM, 17296 standard on Additive Manufacturing (AM) Technologies

[22] Deckers J, Vleugels J and Kruth J P 2004 Additive Manufacturing of Ceramics: A Review. *J. Ceram. Sci. Tech.*, pp. 1-51

[23] Kruth J P, Levy G, Klocke F and Childs T H C 2007 Consolidation phenomena in laser and powder-bed based layered manufacturing. *Annals of the CIRP*. 56: 730–759

[24] Mahale T H 2009 *Electron Beam Melting of advanced materials and structures*. PhD thesis, North Carolina State University

[25] Raabe D, Ponge D, Dmitrieva O and Sander B 2009 Nano-precipitate hardened 1.5 GPa steels with unexpected high ductility. *Scr. Mater.* 60: 1141–1144

[26] Herbig M, Raabe D, Li Y J, Choi P, Zaefferer S and Goto S 2014 Atomic-scale quantification of grain boundary segregation in nanocrystalline material. *Phys. Rev. Lett.* 112: 126103

[27] Lejcek P 2010 Grain boundary segregation in metals. Springer Verlag, Berlin, Heidelberg

[28] Felfer P J, Alam T, Ringer S P and Cairney J M 2012 A reproducible method for damage- free site-specific preparation of atom probe tips from interfaces. *Microsc. Res. Techniq.* 75: 484–491

[29] Toji Y, Matsuda H, Herbig M, Choi P P and Raabe D 2014 Atomic-scale analysis of carbon partitioning between martensite and austenite by atom probe tomography and correlative transmission electron microscopy. *Acta Mater.* 65: 215–228

[30] Gault B, Moody M P, Cairney J M and Ringer S P 2012 Atom probe crystallography. *Mater. Today.* 15: 378–386

[31] Williams C B 2008 *Design and development of a layer-based Additive Manufacturing process for the realization of metal parts of designed mesostructured*. PhD thesis, Georgia Institute of Technology

[32] Sirringhaus H and Shimoda T 2003 Inkjet Printing of functional materials. *Mater. Res. Soc. Bull. Inkjet Print. Func. Mater.* 28: 802–806

[33] Ebert J, Özkol E, Zeichner A, Uibel K, Weiss Ö, Koops U, Telle R and Fischer H 2009 Direct Inkjet Printing of dental prostheses made of zirconia. *J. Dent. Res.* 88: 673–676

[34] Özkol E, Wätjen M, Bermejo R, Deluca M, Ebert J, Danzer R and Telle R 2010 Mechanical characterisation of miniaturised direct inkjet printed 3Y-TZP specimens for microelectronic applications. *J. Eur. Ceram. Soc.* 30: 3145–3152

[35] Hon K K B, Li L and Hutchings I M 2008 Direct writing technology - advantages and developments. *CIRP Ann. Manuf. Technol.* 57: 601–620

[36] Sukeshini M, Meisenkothen F, Gardner P and Reitz T L 2013 Aerosol Jet Printing of functionally graded SOFC anode interlayer and microstructural investigation by low voltage Scanning Electron Microscopy. *J. Power Sourc.* 224: 295–303

[37] Grida I and Evans J R G 2003 Extrusion freeforming of ceramics through fine nozzles. *J. Eur. Ceram. Soc.* 23: 629–635

[38] Yardimci M A and Güçeri S 1996 Conceptual framework for the thermal process modelling of fused deposition. *Rapid Prototyp. J.* 2: 26–31

[39] Venkataraman N, Rangarajan S, Matthewson M J, Harper B, Safari A, Danforth S C, Wu G, Langrana N, Guceri S and Yardimci A 2000 Feedstock material property—process relationships in Fused Deposition of Ceramics (FDC). *Rapid Prototyp. J.* 6: 244–253

[40] Miranda P, Siaz E, Gryn K and Tomsia A P 2006 Sintering and Robocasting of beta-tricalcium phosphate scaffolds for orthopaedic applications. *Acta Biomaterialia* 2: 457–466

[41] Bocanegra-Bernal M H and Matovic B 2009 Dense and near-net-shape fabrication of Si3N4 ceramics. *Mater. Sci. Eng. A.* 500: 130–149

[42] Cai K, Roman-Manso B, Smay J E, Zhou J, Osendi M I, Belmonte M and Miranzo P 2012 Geometrically complex silicon carbide structures fabricated by Robocasting. *J. Am. Ceram. Soc.* 95: 2660–2666

[43] de Hazan Y, Thänert M, Trunec M and Misak J 2012 Robotic deposition of 3D nanocomposite and ceramic fiber architectures via UV curable colloidal inks. *J. Eur. Ceram. Soc.* 32: 1187–1198

[44] Li J P, Habibovic P, van den Doel M, Wilson C E, de Wijn J R, van Blitterswijk C A and de Groot K 2007 Bone ingrowth in porous titanium implants produced by 3D fiber deposition. *Biomaterials.* 28: 2810–2820

[45] King B H, Dimos D, Yang P and Morissette S L 1999 Direct-write fabrication of integrated, multilayer ceramic components. *J Electroceram.* 3: 173–178

[46] Travitzky N, Bonet A, Dermeik B, Fey T, Filbert-Demut I, Schlier L, Schlordt T and Greil P 2014 Additive manufacturing of ceramic-based materials. *Adv. Eng. Mater.* 16: 729–754

[47] Leu M C, Pattnaik S and Hilmas G E 2012 Investigation of Laser Sintering for freeform fabrication of zirconium diboride parts. *J Virtual Phys. Prototyp.* 7: 25–36

[48] Huang T, Mason M S, Hilmas G E and Leu M C 2006 Freeze-form extrusion fabrication of ceramic parts. *Int. J. Virtual Phys. Prototyp.* 1: 93–100

[49] McMillen D, Li W, Leu M C, Hilmas G E and Watt J 2016 designed extrudate for additive manufacturing of zirconium diboride by ceramic on-demand extrusion. Solid Freeform Fabrication. In: *Proceedings of the 26th Annual International Solid Freeform Fabrication Symposium – An Additive Manufacturing Conference*

[50] Feilden E, Glymond D, Saiz E and Vandeperre L 2019 High temperature strength of an ultra high temperature ceramic produced by additive manufacturing. *Ceramics Int.* 45: 18210–18214

[51] Balla V K, Bose S and Bandyopadhyay A 2008 Processing of bulk alumina ceramics using Laser Engineered Net Shaping. *Int. J. Appl. Ceram. Technol.* 5: 234–242

[52] Wang F, Mei J, Jiang H and Wu X 2007 Laser fabrication of Ti6Al4V/TiC composites using simultaneous powder and wire feed. *Mater. Sci. Eng. A.* 445: 461–466

[53] Chen A N, Wu J M, Liu K, Chen J Y, Xiao H, Chen P, Li C H and Shi Y S 2017 High-performance ceramic parts with complex shape prepared by selective laser sintering: a review. *Adv. Appl.Ceram.* 117: 100–117

[54] Dierkes S, Faber A J, Wilkes J, Welters M P M, Meiners W and Wissembach K 2011 International patent WO2011/018463A1. Ceramic or glass- ceramic article and methods for producing such article

[55] Lakiza S M and Lopato L M 1997 Stable and metastable phase relations in the system Alumina–Zirconia–Yttria. *J. Am. Ceram. Soc.* 80: 893–902

[56] Tang H H 2002 Direct Laser Fusion to form ceramic parts. *Rapid Prototyp. J.* 8: 284–289

[57] Tang H H Yen H C and Lin W H 2003 On ceramic parts fabricated Rapid Prototyping machine based on Ceramic Laser Fusion, *SFF Symposium*, Texas

[58] Tang H H, Yen H C, Su S M and Lin Z Y 2004 Prospect of making ceramic shell mold by ceramic laser fusion. *SFF Symposium, Texas*

[59] Yen H C and Tang H H 2012 Study on direct fabrication of ceramic shell mold with slurry-based Ceramic Laser Fusion and Ceramic Laser Sintering. *Int. J. Adv. Manuf. Technol.* 60: 1009–1015

[60] Deckard C R, Beaman J J and Darrah J F 1992 Method of producing parts. Patent WO1992008567A1

[61] Lakshminarayan U, Ogrydiziak S, and Marcus HL 1990 Selective Laser Sintering of ceramic materials. SFF Symposium. Texas

[62] Lakshminarayan U and Marcus H L 1991 Microstructural and mechanical properties of Al2O3/P2O3 and Al2O3/B2O3 composites fabricated by selective laser sintering. *SFF Symposium. Texas*

[63] Bertrand P, Bayle F, Combe C, Goeuriot P and Smurov I 2007 Ceramic components manufacturing by Selective Laser Sintering. *App. Surf. Sci.* 254: 989–992

[64] Gahler A and Heinrich J G 2006 Direct Laser Sintering of Al2O3-SiO2 dental ceramic components by layer-wise slurry deposition. *J. Am. Ceram. Soc.* 89: 3076–3080

[65] Bergstörm L 2001 Colloidal processing of ceramics. In: *Handbook of Applied Surface and Colloid Chemistry*. (ed. K. Holmberg). Wiley, New York

[66] Deckers J, Shahzad K, Vleugels J and Kruth J 2012 Isostatic pressing assisted indirect selective laser sintering of alumina components. *Rapid Prototyp. J.* 18: 409–419

[67] Heinrich J G 2009 LSD-based Selective Laser Sintering. CFI. *Ceramic Forum International/Berichte der DKG (Deutsche Keramische Gesellschaft)* 86: E129–E130

[68] Tian X, Günster J, Melcher J, Li D and Heinrich J G 2009 Process parameters analysis of direct Laser Sintering and post treatment of porcelain components using Taguchi's method. *J. Eur. Ceram. Soc.* 29: 1903–1915

[69] Tian X, Li D and Heinrich J G 2012 Rapid Prototyping of porcelain products by Layer-wise Slurry Deposition (LSD) and direct Laser Sintering. *Rapid Prototyp. J.* 18: 362–373

[70] Tian X, Sun B, Heinrich J G and Li D 2010 Stress relief mechanism in layer-wise laser directly sintered porcelain ceramics. *Mater. Sci. Eng. A.* 527: 1695–1703

[71] Heinrich J G, Gahler A, Günster J, Schmücker M, Zhang J, Jiang D and Ruan M 2007 Microstructural evolution during direct Laser Sintering in the Al2O3-SiO2 system. *J. Mater. Sci.* 42: 5307–5311

[72] Klocke F, Derichs C, Ader C and Demmer A 2007 Investigations on Laser Sintering of ceramic slurries. *Prod. Eng. Res. Devel.* 1: 279–284

[73] Regenfuss P, Streek A, Hartwig L, Klötzer S, Brabant T, Horn M, Ullmann F, Ebert R and Exner H 2007 Material depending mechanisms in Laser Micro Sintering. In: *Proceedings of the 5th LANE conference*, Erlangen, pp. 403-418

[74] Exner H, Regenfuss P, Ebert R, Hartwig L, Streek A, Klötzer S and Horn M 2006 Lasermikrosintern von keramischen Materialien. *RTejournal - Forum für Rapid Technologie.* 3: 1–18

[75] Regenfuss P, Streek A, Hartwig L, Horn M, Klötzer S, Ebert R and Exner H 2008 Freeform fabrication of dental inlays by Laser Micro-Sintering. *Laser User Magazine.* 52: 36–38

[76] Regenfuss P, Streek A, Ullmann F, Hartwig L, Horn M, Kühn C, Ebert R, and Exner H 2008 Laser Microsintering - reaction models and results. *cfi/Berichte DKG*. 85: 65-72

[77] Regenfuss P, Streek A, Ullmann F, Kühn C, Hartwig L, Horn M, Ebert R and Exner H 2008 Laser Micro Sintering of ceramic materials, part 2. *Interceram.* 57: 6–9

[78] Deckers J, Meyers S, Wijremblewski B, Kruth J P and Vleugels J 2014 Direct selective laser sintering/melting of high density alumina powder layers at elevated temperatures', 8th International Conference on Photonic Technologies LANE. Fürth. *Physics Procedia*, pp. 117- 124

[79] Deckers J, Meyers S, Wijremblewski B, Vleugels J and Kruth J P 2014 Direct selective laser sintering/melting of fine grained alumina with a novel experimental setup. *Materials Science and Technology: special issue on 3D printing*

[80] Wijremblewski B 2013 *Testing an experimental setup for the selective laser sintering of technical ceramics (Master thesis)*. PhD thesis. KU Leuven

[81] Vasiliauskaite E, Van Paepegem W, Deckers J P, Vermandel M, Forward M and Plasschaert F 2020 Additive manufacturing of ankle-foot Orthosis with predefined ankle stiffness—a case report. *J. Prosthet. Orthot.* 32: 310–318

[82] Faes M, Vleugels J, Vogeler F and Ferraris E 2016 Extrusion-based additive manufacturing of ZrO2 using photoinitiated polymerization. *CIRP J. Manuf. Sci. Technol.* 14: 28–34

[83] Bertrand P, Yadroitsev I and Smurov I 2004 Prototypage rapide et fabrication directe par laser d'objets multimatériaux multifonctionnels. Dixième assisses Europ. de Prototypage Rapide, Paris

[84] Birmingham B R and Marcus H L 1995 Solid Freeform Fabrication of silicon nitride shapes by Selective Laser Reaction Sintering (SLRS). *SFF Symposium*. Texas

[85] Klocke F and Wirtz H 1997 Selective Laser Sintering of ceramics, In: *Laser Assisted Net Shape Engineering (LANE) conference*. Erlangen

[86] Tang HH 1993 Ceramic Laser Sintering - optimization of ceramic Rapid Prototyping Technical report of the National Taipei University of Technology in Taiwan

[87] Barlow J W and Vail N K, International patent WO 93/19019: Producing high-temperature parts by low-temperature sintering. 86

[88] Liu Z H, Nolte J J, Packard J I, Hilmas G, Dogan F and Leu M C 2007 Selective Laser Sintering of high density alumina ceramic parts, In: *Proceedings of the 35th MATADOR conference*, Taipei (Taiwan), pp. 351-354

[89] Regenfuss P, Streek A, Hartwig L, Klötzer S, Brabant T, Horn M, Ullmann F, Ebert R and Exner H 2007 Material depending mechanisms in Laser Micro Sintering, In: *Proceedings of the 5th LANE conference*, Erlangen, pp. 403-418

[90] Shishkovsky I, Yadroitsev I, Bertrand P and Smurov I 2007 Alumina- zirconium ceramics synthesis by Selective Laser Sintering/Melting. *Appl. Surf. Sci.* 254: 966–970

[91] Leu M C, Adamek EB, Huang T, Hilmas G E and Dogan F 2008 Freeform fabrication of zirconium diboride parts using selective laser sintering. *SFF Symposium. Texas*

[92] Leu M C, Pattnaik S and Hilmas G E 2010 Optimization of selective laser sintering process for fabrication of zirconium diboride parts. *SFF Symposium, Texas*

[93] Shahzad K 2013 *Powder-based indirect selective laser sintering of ceramics* (Doctoral thesis), PhD thesis, KU Leuven

[94] Deckers J 2013 *Selective Laser Sintering and Melting as Additive Manufacturing Methods to Produce Alumina Parts; '3D printing' of Ceramics* (Doctoral thesis)', PhD thesis, KU Leuven, 2013

[95] Cardon L, Deckers J, Verberckmoes A, Ragaert K, Delva L, Shahzad K, Vleugels J and Kruth J 2013 Polystyrene-coated alumina powder via dispersion polymerization for indirect selective laser sintering applications. *J. Appl. Polym. Sci.* 128: 2121–2128

[96] Gill T J and Hon K K B 2004 Experimental investigations into the selective laser sintering of silicon carbide polyamide composites. *Proc. IMechE Part B J. Eng. Manuf.* 218: 1249–1256

[97] Stucker B E, Bradley W L, Norasetthekul S and Eubank P T 1995 The Production of Electrical Discharge Machining Electrodes Using SLS: Preliminary Results, In: *Proceedings of Solid Freeform Fabrication Symposium*, Austin, Texas, pp. 278-286

[98] Stucker B E, Bradley W L, Eubank P T, Norasetthekul S and Bedri B 1997 Zirconium Diboride/Copper EDM Electrodes From Selective Laser Sintering, In: *Proceedings of Solid Freeform Fabrication Symposium*, Austin. Texas, pp. 257-265

[99] Sun C N and Gupta M C 2008 Laser Sintering of ZrB_2. *J. Am. Ceramic Soc.* 91: 1729–1731

[100] Evans R S, Bourell D L, Beaman J J and Campbell M I 2005 Rapid manufacturing of silicon carbide composites. *Rapid Prototyp. J.* 11: 37–40

[101] Yen H C, Tang H H and Wu C H 2011 Improving staircase effect in the process of Ceramic Laser Gelling. *Adv. Mater. Res.* 284–286: 43–47

[102] Liu F H and Liao Y S 2010 Fabrication of inner complex ceramic parts by Selective Laser Gelling. *J. Eur. Ceram. Soc.* 30: 3283–3289

[103] Liu F H 2011 Manufacturing porous multi-channel ceramic by Laser Gelling. *Ceram. Int* 37: 2789–2794

[104] Griffith M L and Halloran J W 1996 Freeform Fabrication of Ceramics via Stereolithography. *J. Am. Ceram. Soc.* 79: 2601–2608

[105] Halloran J W, Tomeckova V, Gentry S, Das S, Cilino P, Yuan D, Guo R, Rudraraju A, Shao P, Wu T, Alabi T R, Baker W, Legdzina D, Wolski D, Zimbeck W R and Long D 2011 Photopolymerization of powder suspensions for shaping ceramics. *J. Eur. Ceram. Soc.* 31: 2613–2619

[106] Wang J C 2013 A novel fabrication method of high strength alumina ceramic parts based on solvent-based slurry stereolithography and sintering. *Int. J. Precis. Eng. Manuf.* 14: 485–491

[107] de Hazan Y, Heinecke J, Weber A and Graule T 2009 High solids loading ceramic colloidal dispersions in UV curable media via comb- polyelectrolyte surfactants. *J. Colloid Interface Sci.* 337: 66–74

[108] Jacobs P F 1992 Rapid prototyping & manufacturing - fundamentals of stereolithography. *Society of Manufacturing Engineers*, pp. 29-33

[109] Liu X, Zou B, Xing H and Huang C 2020 The preparation of ZrO_2-Al_2O_3 composite ceramic by SLA-3D printing and sintering processing. *Ceram. Int.* 46: 937–944

[110] Bertsch A, Jiguet S and Renaud P 2004 Microfabrication of ceramic components by microstereolithography. *J. Micromech. Microeng.* 14: 197–203

[111] Nold A, Zeiner J, Assion T and Clasen R 2010 Electrophoretic deposition as Rapid Prototyping method. *J. Eur. Ceram. Soc.* 30: 1163–1170

[112] Aramiana A, Razavi S M J, Sadeghiana Z and Bertob F 2020 A review of additive manufacturing of cermets. *Addit. Manuf.* 33: 1–17

[113] Uhlmann E, Bergmann A and Gridin W 2015 Investigation on additive manufacturing of tungsten carbide-cobalt by selective laser melting. *Procedia Cirp.* 35: 8–15

[114] Simchi A 2006 Direct laser sintering of metal powders: Mechanism, kinetics and microstructural features. *Mater. Sci. Eng. A.* 428: 148–158

[115] Xiong Y, Smugeresky J E, Lavernia E and Schoenung J M 2008 Processing and micro- structure of WC-CO cermets by laser engineered net shaping. In: *19th* Annu. *Int. Solid Free. Fabr. Symp. SFF*

[116] Enneti R K and Prough K C 2019 Wear properties of sintered WC-12%Co processed via Binder Jet 3D Printing (BJ3DP). *Int. J. Refract. Met. Hard Mater.* 78: 228–232

[117] Lengauer W, Duretek I, Fürst M, Schwarz V, Gonzalez-Gutierrez J, Schuschnigg S, Kukla C, Kitzmantel M, Neubauer E, Lieberwirth C and Morrison V 2019 Fabrication and properties of extrusion-based 3D-printed hardmetal and cermet components. *Int. J. Refract. Met. Hard Mater.* 82: 141–149

[118] Zhang X, Guo Z, Chen C and Yang W 2018 Additive manufacturing of WC-20Co compo- nents by 3D gel-printing. *Int. J. Refract. Met. Hard Mater.* 70: 215–223

[119] Krakhmalev P and Yadroitsev I 2014 Microstructure and properties of intermetallic com- posite coatings fabricated by selective laser melting of Ti-SiC powder mixtures. *Intermetallics.* 46: 147–155

[120] Khmyrov R S, Safronov V A and Gusarov A V 2017 Synthesis of nanostructured WC-Co hardmetal by selective laser melting. *Procedia IUTAM.* 23: 114–119

[121] Khmyrov R S, Shevchukov A P, Gusarov A V and Tarasova T V 2017 Phase composition and microstructure of WC-Co alloys obtained by selective laser melting, *Mech. Ind*. 18

[122] Grigoriev S, Tarasova T, Gusarov A, Khmyrov R and Egorov S 2019 Possibilities of manufacturing products from cermet compositions using nanoscale powders by additive manufacturing methods. *Materials (Basel).* 12

[123] Campanelli S L, Contuzzi N, Posa P and Angelastro A 2019 Printability and microstructure of selective laser melting of WC/Co/Cr powder, *Materials (Basel)*. 12

[124] Domashenkov A, Borbély A and Smurov I 2016 Structural modifications of WC/Co nano- phased and conventional powders processed by selective laser melting. *Mater. Manuf. Process.* 32: 93–100

[125] Gu D and Shen Y 2008 Direct laser sintered WC-10Co/Cu nanocomposites. *Appl. Surf. Sci.* 254: 3971–3978

[126] Kumar S 2018 Process chain development for additive manufacturing of cemented carbide. *J. Manuf. Process.* 34: 121–130

[127] Gu D and Meiners W 2010 Microstructure characteristics and formation mechanisms of in situ WC cemented carbide based hard metals prepared by Selective Laser Melting. *Mater. Sci. Eng. A.* 527: 7585–7592

[128] Gu D D, Shen Y F, Dai P and Yang M C 2006 Microstructure and property of sub-micro WC-10%Co particulate reinforced Cu matrix composites prepared by selective laser sintering. *Trans. Nonferrous Met. Soc. China (English Ed.)* 16: 357–362

[129] Xiong Y, Smugeresky J E, Ajdelsztajn L and Schoenung J M 2008 Processing and Microstructure of WC-Co cermets by laser engineering net shaping. *Mater. Sci. Eng. A*. 493: 261–266

[130] Sahasrabudhe H and Bandyopadhyay A 2016 Additive Manufacturing of reactive in situ Zr based ultra-high temperature ceramic composites. *JOM*. 68: 822–830

[131] Xiong Y, Smugeresky J E and Schoenung J M 2009 The influence of working distance on laser deposited WC-Co. *J. Mater. Process. Technol.* 209: 4935–4941

[132] Xiong Y, Kim M, Seo O, Schoenung J M and Kang S 2010 (Ti, W)C–Ni cermets by laser engineered net shaping. *Powder Metall.* 53: 41–46

[133] Li Y, Bai P, Wang Y, Hu J and Guo Z 2009 Effect of Ni contents on the microstructure and mechanical properties of TiC-Ni cermets obtained by direct laser fabrication. *Int. J. Refract. Met. Hard Mater.* 27: 552–555

[134] Prichard P D and Collins G B 2018 Cemented carbide powders for additive manufacturing, U.S. Patent Application 15

[135] Enneti R K and Prough K C 2019 Effect of binder saturation and powder layer thickness on the green strength of the binder jet 3D printing (BJ3DP) WC-12 % Co powders. *Int. J. Refract. Metals Hard Mater*. 84: 104991

[136] Flon J D 2019 Three dimensional printing of cermet or cemented carbide, U.S. Patent Application 16

[137] Reyes M and Neville A 2003 Degradation mechanisms of Co-based alloy and WC metal-matrix composites for drilling tools offshore. *Wear.* 255: 143–156

[138] Cramer C L, Aguirre TG, Wieber N R, Lowden R A, Trofimov A A, Wang H, Yan J, Paranthaman M P and Elliott A M 2019 Binder jet printed WC infiltrated with pre-made melt of WC and Co. *Int. J. Refract. Met. Hard Mater.* 105137

[139] Cramer C L, Nandwana P, Lowden R A and Elliott A M 2019 Infiltration studies of additive manufacture of WC with Co using binder jetting and pressureless melt method. *Addit. Manuf.* 28: 333–343

[140] Cramer C L, Wieber N R, Aguirre T G, Lowden R A and Elliott A M 2019 Shape retention and infiltration height in complex WC-Co parts made via binder jet of WC with subsequent Co melt infiltration, *Addit. Manuf*. 29. 100828

[141] Michael K, Walter L, Ivica D and Viktoria S 2018 Potential of extrusion based 3D-printed hardmetal and cermet parts. *World Congr. Powder Metall*

[142] Satish Prakash K, Nancharaih T and Subba Rao V V 2018 Additive manufacturing techniques in manufacturing—an overview. *Mater. Today Proc.* 5: 3873–3882

[143] Gao W *et al*. 2015 The status, challenges, and future of additive manufacturing in Engineering. *Comput-Aided Des.* 69: 65–89

[144] Zocca A, Colombo P, Gomes C M and Günster J 2015 Additive manufacturing of ceramics: issues, potentialities, and opportunities. *J. Am. Ceram. Soc.* 98: 1983–2001

[145] Tang Y, Henderson C L, Muzzy J and Rosen D W 2004 Stereolithography cure process modeling using acrylate resin. In: *Proceedings of the International Solid Freeform Fabrication Symposium*, Austin, TX

[146] Turner B N and Gold S A 2015 A review of melt extrusion additive manufacturing processes: II. Materials, dimensional accuracy, and surface roughness. *Rapid Prototyp. J.* 21: 250–261

[147] Liu H, Su H, Shen Z, Wang E, Zhao D, Guo M, Zhang J, Liu L and Fu H 2018 Direct formation of Al2O3/GdAlO3/ZrO2 ternary eutectic ceramics by selective laser melting: Microstructure evolutions. *J. Eur. Ceram. Soc.* 38: 5144–5152

[148] Triantafyllidis D, Li L and Stott F H 2003 Mechanisms of porosity formation along the solid/liquid interface during laser melting of ceramics. *Appl. Surf. Sci.* 208–209: 458–462

[149] Cao S, Gu D and Shi Q 2017 Relation of microstructure, microhardness and underlying thermodynamics in molten pools of laser melting deposition processed TiC/Inconel 625 composites. *J. Alloys Compd.* 692: 758–769

[150] Larrea A, de la Fuente G F, Merino R I and Orera V M 2002 ZrO2-Al2O3 eutectic plates produced by laser zone melting. *J. Eur. Ceram. Soc.* 22: 191–198

[151] Guessasma S, Zhu Zhang W and J, Belhabib S and Nouri H, 2015 Challenges of additive manufacturing technologies from an optimisation perspective. *Int. J. Simul. Multisci. Des. Optim.* 6: A9

[152] Guessasma S, Belhabib S and Nouri H 2015 Significance of pore percolation to drive anisotropic effects of 3D printed polymers revealed with X-ray l-tomography and finite element computation. *Polymer.* 81: 29–36

[153] Liu H, Su H, Shen Z, Zhao D, Liu Y, Guo M, Guo Y, Zhang J, Liu L and Fu H 2019 Effect of scanning speed on the solidification process of Al2O3/GdAlO3/ZrO2 eutectic ceramics in a single track by selective laser melting. *Ceram. Int.* 45: 17252–17257

[154] Liu Q, Danlos Y, Song B, Zhang B, Yin S and Liao H 2015 Effect of high-temperature preheating on the selective laser

melting of yttria-stabilized zirconia ceramic. *J. Mater. Process. Technol.* 222: 61–74

[155] Liu H, Su H, Shen Z, Zhao D, Liu Y, Guo Y, Guo H, Guo M, Xie K, Zhang J and Liu Land Fu H 2021 One-step additive manufacturing and microstructure evolution of melt-grown Al2O3/GdAlO3/ZrO2 eutectic ceramics by laser directed energy deposition. *J. Eur. Ceram. Soc.* 41: 3547–3558

[156] Fan Z, Zhao Y, Tan Q, Mo N, Zhang M X, Lu M and Huang H 2019 Nanostructured Al2O3-YAG-ZrO2 ternary eutectic components prepared by laser engineered net shaping. *Acta Materialia.* 170: 24–37

[157] Ludwig A and Leibbrandt S 2004 Generalised 'Jackson–Hunt' model for eutectic solidification at low and large Peclet numbers and any binary eutectic phase diagram. *Mater. Sci. Eng. A.* 375–377: 540–546

[158] Wang X, Zhong Y, Sun Q, Qi D, Yan F, Xian Q, Wang D, Du K and Wang J 2019 Competitive growth of Al2O3/YAG/ZrO2 eutectic ceramics during directional solidification: effect of interfacial energy. *J. Am. Ceram. Soc.* 102: 2176–2186

[159] Wang X, Wang J, Sun L, Zhang H, Wang L, Lou L and Zhang J 2015 Microstructure evolution of $Al_2O_3/Y_3Al_5O_{12}$ eutectic crystal during directional solidification. *Scripta Mater.* 108: 31–34

[160] Wang X, Zhong Y, Sun Q, Li Y, Zhang W, Qi D, Wang D and Jiang B 2018 Crystallography and interfacial structure in a directionally solidified Al 2 O 3/Y 3 Al 5 O 12/ZrO $_2$ eutectic crystal. *Scripta Mater.* 145: 23–27

[161] Foster B K, Reutzel E W, Nassar A R, Dickman C J and Hall B T 2015 A brief survey of sensing for metal-based powder bed fusion additive manufacturing. Dimensional Optical Metrology and Inspection for Practical Applications Iv. 9489: 94890B-1–94890B-9

[162] Furumoto T, Koizumi A, Alkahari M R, Anayama R, Hosokawa A and Tanaka and Ueda R T, 2015 Permeability and strength of a porous metal structure fabricated by additive manufacturing. *J. Mater.Process. Technol.* 219: 10–16

[163] Chianrabutra S, Mellor B G and Yang S 2014 A Dry Powder Material Delivery Device for Multiple Material Additive Manufacturing, Solid Freeform Fabrication Symposium. In: *Proceedings of the University of Texas at Austin, Austin, Texas*

[164] Akram J, Chalavadi P, Pal D and Stucker B 2018 Understanding grain evolution in additive manufacturing through modelling. *Addit. Manuf.* 21: 255–268

[165] Raghavan N, Simunovic S, Dehoff R, Plotkowski A, Turner J, Kirka M and Babu S 2017 Localized melt-scan strategy for site specific control of grain size and primary dendrite arm spacing in electron beam additive manufacturing. *Acta Materialia.* 140: 375–387

[166] Yang S and Evans J R G 2004 A multi-component powder dispensing system for three dimensional functional gradients. *Mater. Sci. Eng. A.* 379: 351–359

[167] Halloran J W 2016 Ceramic stereolithography: additive manufacturing for ceramics by photopolymerization. *Annu. Rev. Mater. Res.* 46: 19–40

[168] Yang L and Miyanaji H 2017 Ceramic Additive Manufacturing: A Review of current status and challenges. Solid Freeform Fabrication. In: *Proceedings of the 28th Annual International Solid Freeform Fabrication Symposium – An Additive Manufacturing Conference*; pp. 652-679

[169] Hinczewski C, Corbel S and Chartier T 1998 Ceramic suspensions suitable for stereolithography. *J. Euro. Ceram. Soc.* 18: 583–590

[170] Bae C J and Halloran J W 2011 Integrally cored ceramic mold fabricated by ceramic stereolithography. *Int. J. Appl. Ceram. Technol.* 8: 1255–1262

[171] Blackburn S and Wilson D I 2008 Shaping ceramics by plastic processing. *J. Eur. Ceram. Soc.* 28: 1341–1351

[172] Woodward I, Purssell C P, Billson D R, Hutchins D A and Leigh S J 2015 Additively- manufactured piezoelectric devices. *Phys. Status Solidi A.* 212: 2107–2113

[173] Hall E O 1951 The deformation and ageing of mild steel: III discussion of results. *Proc. Phys. Soc. London Sect. B.* 64: 747

[174] Qian B and Shen Z 2013 Laser sintering of ceramics. *J. Asian Ceram. Soc* 1: 315–321

[175] Petch N J 1953 The cleavage strength of polycrystals. *J. Iron Steel Inst. London.* 174: 25

[176] Lipowsky P, Bowick M and Meinke J *et al*. 2005 Direct visualization of dislocation dynamics in grain-boundary scars. *Nature Mater.* 4: 407–411

[177] Shan Z, Stach E A, Wiezorek J M K, Knapp J A, Follstaedt D M, Mao S X, Grain Boundary-Mediated Plasticity in Nanocrystalline Nickel. *Science.* 305: 654-657

[178] Koch C C, Morris D G, Lu K and Inoue A 1999 Ductility of nanostructured materials. *MRS Bull.* 24: 54

[179] Weertman R, Farkas D, Hemker K, Kung H, Mayo M, Mitra R and Van Swygenhoven H 1999 Structure and mechanical behavior of bulk nanocrystalline materials. *MRS Bull.* 24: 44

[180] Masumura R A, Hazzledine P M and Pande C S 1998 Yield stress of fine grained materials. *Acta Mater.* 46: 4527

[181] Van Swygenhoven H and Caro A 1997 Plastic behavior of nanophase Ni: A molecular dynamics computer simulation. *Appl. Phys. Lett.* 71: 1652

[182] Watanabe T 2011 Grain boundary engineering: historical perspective and future prospects. *J. Mater. Sci.* 46: 4095–4115

[183] Watanabe T and Tsurekawa S 2004 Toughening of brittle materials by grain boundary engineering. *Mater. Sci. Eng. A.* 387–389: 447–455

[184] Leung C L A, Marussi S and Atwood R C *et al*. 2018 In situ X-ray imaging of defect and molten pool dynamics in laser additive manufacturing. *Nat. Commun.* 9: 1355

[185] Roca J B, Vaishnav P and Fuchs E *et al*. 2016 Policy needed for additive manufacturing. *Nat. Mater.* 15: 815–818

[186] Chen Z, Li Z, Li J, Liu C, Lao C, Fu Y, Liu Li Y, Wang P and He Y 2019 3D printing of ceramics: A review. *J. Eur. Ceram. Soc.* 39: 661–687

[187] Hwa L C, Rajoo S, Noor A M, Ahmad N and Uday M B 2017 Recent advances in 3D printing of porous ceramics: A review. *Curr. Opinion Solid State Mater. Sci.* 21: 323–347

[188] Mansfield B, Torres S, Yu T and Wu D 2019 A Review on Additive Manufacturing of Ceramics. In: *Proceedings of the ASME 2019 14th International Manufacturing Science and Engineering Conference*. In: *Volume 1: Additive Manufacturing; Manufacturing Equipment and Systems;*

Bio and Sustainable Manufacturing. Erie, Pennsylvania, USA

[189] Deng D and Chen Y 2014 Origami-based self-folding structure fabrication based on 3D printing on polystyrene film, In: *ASME mechanism and robotics conference, DETC2014-34901, Buffalo (NY, USA)*

[190] Ashby M, Gibson L, Wegst U and Olive R 1995 The mechanical properties of natural materials. I. Material property charts. *Proc. R. Soc. Lond. Ser. A*. 450: 123–140

[191] Fratzl P, Gupta H, Paschalis E and Roschger P 2004 Structure and mechanical quality of the collagen-mineral nano-composite in bone. *J. Mater. Chem.* 14: 2115–2123

[192] Espinosa H, Rim J, Barthelat F and Buehler M 2009 Merger of structure and material in nacre and bone—perspective on de novo biomimetic materials. *Prog. Mater. Sci.* 54: 1059–1100

[193] Sutherland I 1964 Sketchpad: a man–machine graphical communication system. In: *Proceedings of the SHARE design automation workshop*, pp. 6329–46

[194] Olsen L, Samavati F, Sousa M and Jorge J 2008 Sketch-based modeling: A survey. *Comput. Graph.* 33: 85–103

[195] Contero M, Naya F, Jorge J and Conesa J 2003 CIGRO: A minimal instruction set calligraphic interface for sketch-based modeling. *Lecture Notes Comput. Sci.* 2669: 549–558

[196] Yang C, Sharon D and van de Panne M 2005 Sketch-based modeling of parameterized objects. In: *Proceedings of eurographics workshop on sketch-based interfaces and modeling, SBIM'05*

[197] Lee J and Funkhouser T 2008 Sketch-based search and composition of 3D models. In: *Proceedings of eurographics workshop on sketch-based interfaces and modelling. SBIM'08*